



Water entry of an elastic conical shell

T.I. Khabakhpasheva^{1,†}, A.A. Korobkin¹ and S. Malenica²

¹School of Mathematics, University of East Anglia, Norwich NR4 7TJ, UK

²Bureau Veritas, La Defense, Paris, France

(Received 15 August 2023; revised 9 November 2023; accepted 25 December 2023)

The axisymmetric problem of a conical shell impact onto an inviscid and incompressible liquid of infinite depth is studied. The shell is thin, and its deadrise angle is small. The problem is inertia dominated. Gravity, surface tension and viscous effects are not taken into account. The hydrodynamic loads acting on the shell and the shell displacements are determined at the same time. The model by Scolan (*J. Sound Vib.*, vol. 277, issue 1–2, 2004, pp. 163–203) is used to find the flow and hydrodynamic pressure caused by the shell impact. This model is based on the Wagner theory of water impact, which was generalised to axisymmetric problems of hydroelastic slamming. Dry and wet modes of the conical shell, as well as the corresponding frequencies, are calculated. It is shown that a conical shell can be approximated by a circular plate only for a very small deadrise angle. Deflections and strains in the conical shell during the impact stage, when the wetted part of the shell increases at high rate, as well as the hydrodynamic loads, are determined and analysed.

Key words: wave–structure interactions, general fluid mechanics

1. Introduction

Water impact of thin-walled structures is of practical importance in many applications. Slamming of ships, ditching of aircraft and wave impacts onto offshore platforms are examples of such applications. A structure is quickly wetted during water impact if the curvature of the structure surface is small. As a result, the hydrodynamic loads over the wetted area of the structure can be high enough to deform the structure and even to damage it. One needs to know how the impact conditions are related to the magnitude of the impact loads and to the level of stresses in the structure. This problem of hydroelasticity is complicated because, in the most dangerous conditions, the structural deformations and the loads should be determined at the same time, the contact region between the structural surface and the liquid is unknown in advance and should be determined as part of the solution, the flow is three-dimensional.

† Email address for correspondence: t.khabakhpasheva@uea.ac.uk

1.1. Motivation

Hydrodynamic pressures during the impact are high and sensitive to the local details of the impact conditions. The impact velocity is of course an important parameter but, as far as the extreme localised impact pressures are of concern, the relative local geometry between the fluid and the body surface has significant influence on the pressures. This can be illustrated with the case of a two-dimensional wedge which impacts the initially flat water surface with a constant speed V . The relative impact geometry is defined by a single parameter which is the wedge deadrise angle β . For this problem with a small deadrise angle, a well-known Wagner solution, see Wagner (1932), is appropriate to analyse the pressure behaviour. Under the assumptions of the Wagner theory, it is possible to evaluate the pressure distribution along the wetted part of the wedge analytically. The maximum impact pressure is given then by the following expression,

$$p_{max} = \frac{8\rho V^2}{\pi^2 \tan^2 \beta}, \quad (1.1)$$

where ρ is the water density. The formula (1.1) shows that the maximum pressure dramatically changes even for very small variations of the deadrise angle β . These extreme pressures are usually of short duration, and the affected area is very small. Because of this particular behaviour, it is often not practically possible to correctly estimate the maximum values of the pressure, neither experimentally nor numerically. Indeed, in the case of measurements, the measured pressure value will depend on the size of the pressure gauge and experimental set-up, whereas in numerical simulations it will depend on the mesh size and many other parameters of a numerical algorithm. A very high scatter of measured maximum pressures during water impact was demonstrated in figure 4 of Faltinsen (2000).

It is important to understand that, usually, the results, which are of practical interest, are not the pressures but the structural responses in terms of stresses. In reality, the structural responses are not much affected by localised pressures of short duration, because these pressures are naturally filtered out by the structural dynamics. In order to simulate this type of hydro-structure interactions numerically, fully coupled hydroelastic models are required. Within these models the interaction between the structural dynamics and the hydrodynamic loading is accounted for at each time step of the simulations. The time scale of the structural response determines which physical effects should be included in the model.

In order to illustrate this, the concept of the dynamic amplification factor (DAF) is particularly useful. This factor is defined as the ratio between the real structural response and its quasi-static counterpart. The quasi-static response is defined as the static response of the structure to the hydrodynamic loading precalculated for rigid-body conditions, which means that there is no coupling between the loading and the response. The DAF critically depends on the ratio between the excitation time t_w and the characteristic natural period t_1 of the structure in contact with the liquid. This is illustrated in figure 1 for the case of impact of an elastic wedge onto flat water surface, where the analytical solution under the Wagner assumptions for hydrodynamic part can be found in Khabakhpasheva & Korobkin (2013). Three fundamentally different interaction regimes can be identified: impulsive, dynamic and quasi-static. It can be seen that, in the impulsive regime, significant reduction of the structural response with respect to the quasi-static regime occurs which demonstrates that the localised extreme pressures of short duration are filtered out by the structure. In between the impulsive and quasi-static interaction regime there exists the dynamic interaction regime where the structural response can be amplified.

Water entry of an elastic conical shell

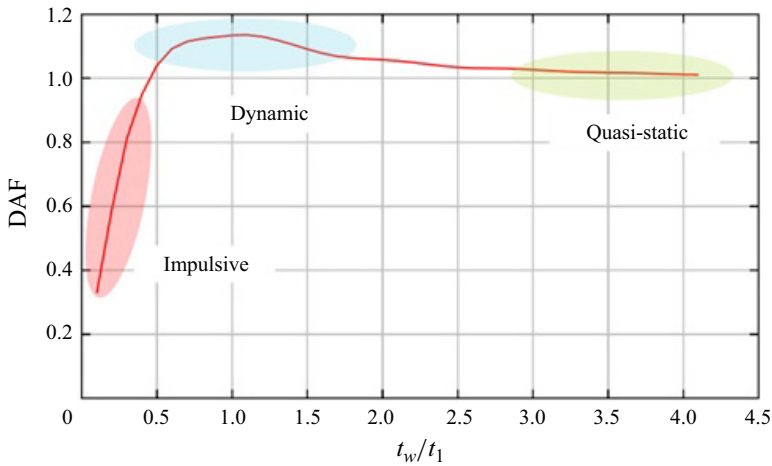


Figure 1. DAF and the different interaction regimes for elastic wedge (from Malenica *et al.* 2022).

All this shows that the fully coupled hydroelastic models need to be used when dealing with the hydro-structure interactions during severe hydrodynamic impacts.

In practical applications, the relative impact geometry is usually very complex, and the three-dimensional conditions need to be modelled, which means that the solution should be fully numerical. Some software providers as well as the research and academic institutions, claim the possibility to perform this kind of simulations. However, to the best of the authors' knowledge, the consistent validation of these models has not yet been provided. The word consistent means here that the theory behind the numerical method is verified and validated for all the above-mentioned interaction regimes. Instead, many comparisons of the numerical and the experimental results were published. The conclusions of these comparisons are usually very enthusiastic even though the numerical and experimental results are most often mixed in the cloud of points which are difficult to properly interpret. At the same time, the conditions in which the experiments are performed, in terms of interaction regimes, are usually not well identified. In the authors' opinion, the best validation material is provided by the analytical solutions of the same problems, when these solutions are available.

The main purpose of this paper is to provide such analytical results for the three-dimensional hydroelastic impact case, knowing that the two-dimensional results were already given in Khabakhpasheva & Korobkin (2013). The model, which is proposed here, allows for highly accurate analytical solution for the water-entry problem of an elastic cone. These results can be directly used for the validation of the general three-dimensional numerical models for all the interaction regimes: impulsive, dynamic and quasi-static. This is particularly important, because the numerical parameters which are relevant for numerical simulations (mesh size and type, time step, shape and size of the computational domain, management of the free surface and others) are strongly dependent on the type of the interaction regime.

1.2. Existing results and approaches

The flow caused by impact can be approximated as two-dimensional for elongated structures using the strip method, see Logvinovich (1972). Then we arrive at two-dimensional coupled problems of hydroelasticity, which can be solved either

numerically (see, for example, Seng (2013) and Malenica *et al.* (2021)) or using the normal mode method within the Wagner theory of water impact (see Khabakhpasheva & Korobkin (2013) and Korobkin & Khabakhpasheva (2006)). Malenica *et al.* (2021) performed numerical calculations of elastic wedge impact onto water surface by coupling the OpenFOAM flow solver to a structural solver which uses a modal superposition approach. The numerical solution was compared with the theoretical solution by the Wagner model for different deadrise angles of the wedge and different impact speeds. The comparison in terms of the maximum deflection and bending stresses was very good, which justified the numerical solution and demonstrated that the Wagner model provides accurate results for deadrise angles up to 25°. The Wagner model of water impact (see Wagner 1932) assumes that the penetration of the body into the liquid and the elevation of the liquid free surface caused by the impact are small compared with the dimensions of the wetted part of the body. This makes it possible to linearise the boundary conditions on both the wetted part of the body and on the free surface and impose these conditions on the initial level of the liquid before the impact. In this model, the flow region is known but the contact line on its boundary, which separates the wetted part of the body and the free surface of the liquid, is unknown in advance and should be determined as part of the solution using the so-called Wagner condition. This condition states that the elevation of the free surface at the contact line matches the position of the entering body at this line. The Wagner condition leads to a transcendental equation with respect to the radius of the contact region as a function of the penetration depth for two-dimensional and axisymmetric bodies. The Wagner model of impact is well investigated for two-dimensional problems with both rigid and elastic bodies.

Three-dimensional problems of hydroelastic impact are much more complicated than the corresponding two-dimensional problems. Water entry of a wedge by hydroelastic orthotropic plate theory was studied by Faltinsen (1999), where hydrodynamic loads were evaluated by the strip theory within the two-dimensional Wagner model and the coupling with the plate theory provided three-dimensional flow effects. Axisymmetric problem of elastic cone impact onto a liquid half space was solved by Grigolyuk & Gorshkov (1971) and Scolan (2004) within the axisymmetric Wagner model of water impact. Grigolyuk & Gorshkov (1971) solved the problem using a nonlinear theory of conical shells approximating the normal displacements of shell elements by quadratic functions. The radius of the wetted part of the cone was approximated by that for a rigid cone supported by an 'equivalent' spring. Inertia of the shell in the tangential direction and the hydrodynamic loads in this direction were neglected. Scolan (2004) approximated an elastic cone with small deadrise angle by a circular elastic plate clamped at the edge and at the centre which corresponds to the tip of the cone. The structure was simplified by Scolan (2004) but the three-dimensional hydrodynamic part of the problem was solved in full details with proper evaluation of the wetted part of the cone at each time instant. Three-dimensional hydroelastic impact onto a floating circular plate was studied by Korobkin & Khabakhpasheva (2022), where the flow was three-dimensional, but the wetted part of the structure was circular and did not change in time.

Axisymmetric problem of elastic cone impact on water was studied numerically and theoretically using the model by Scolan (2004) and the dry modes of the corresponding circular plate by Malenica *et al.* (2022). Describing difficulties with the hydrodynamic solver, they wrote: 'The OpenFoam based numerical CFD models of water impact do not make any particular additional assumptions compared to the classical modeling of the fluid flow in the presence of the free surface. However, the convergence issues and the mesh requirements become much more critical now due to the large velocity of expansion of the

wetted surface and the local sharp free-surface deformation close to the contact points. In the present work the incompressible OpenFoam solver was used together with the Volume of Fluid (VOF) method for free surface capturing'. The finite-element method (FEM) was used to compute deformations of the elastic cone during the water impact. As to the hydroelastic coupling, they mentioned that the fluid loads and local deflections should be transferred between the flow and the structural solvers: 'The strongly-coupled simulations require these two-ways exchanges of loads and deflections to be performed iteratively within each time step until a small tolerance of convergence criteria is satisfied'. Such iterative methods with relaxation are not discussed in the present paper, but will be studied and developed further in the future work of the authors. Numerical procedures, which are based, for example, on OpenFoam and FEM coupling, can be used for general purposes in practice. Development and validation of such procedures would benefit from having highly accurate semi-analytical solutions of three-dimensional problems of hydroelastic slamming.

The method and ideas by Scolan (2004) were used to solve axisymmetric problem of droplet impact onto an elastic plate, see Pegg, Purvis & Korobkin (2018), where a circular plate was built in a rigid substrate. There are still no solutions of truly three-dimensional impact problems for elastic bodies. The axisymmetric problem of rigid cone impact on water was well studied since the pioneering paper by Courant, Shiffman & Spencer (1945), where the self-similar problem of cone impact at a constant speed was studied numerically for a cone with deadrise angle of 30° , by using the numerical method by Wagner (1932) and by several simplified approaches including correction of the wetted region caused by the elevation of the free surface. See also the paper by Shiffman & Spencer (1951), where updated theoretical results from the reports by Courant *et al.* (1945) were published. These numerical and analytical results were confirmed experimentally by Baldwin (1971), see also experimental results for rigid cone impact by Chuang & Milne (1971).

Three-dimensional problem of water impact by a rigid body within the Wagner model was numerically solved by Donguy *et al.* (2001) using the boundary-element method. The wetted part of the entering body was determined by iterations at each time instant. The numerical results for elliptic paraboloid were compared with the analytical results by Scolan & Korobkin (2001). Another numerical method to solve the three-dimensional impact problem was proposed by Tassin *et al.* (2012).

Gazzola & de Lauzon (2008) applied the formulation of Wagner impact problems as a variational inequality (see Korobkin (1982) and Gazzola *et al.* (2005)) to three-dimensional hydroelastic slamming. The numerical results for elastic cone were compared with the theoretical results by Scolan (2004). Note that the formulation of Wagner impact problems as a variational inequality does not require calculations of the position of the wetted part of the entering elastic body.

1.3. Structure of the paper

In the present study, the axisymmetric and hydroelastic Wagner problem of water impact is applied to conical shells of small deadrise angle. The formulation of the problem in dimensionless variables is given in § 2. An important parameter which decreases with decrease of the deadrise angle and increase of the shell thickness is derived. It is shown that a conical shell can be approximated by an equivalent circular plate only for extremely small deadrise angles. Equations for dry and wet modes and their frequencies are derived in § 3 using the modes of a clamped circular plate introduced by Scolan (2004). The hydrodynamic pressure acting over the wetted part of the cone is given by a series with improved convergence. Numerical results for wet and dry modes and frequencies,

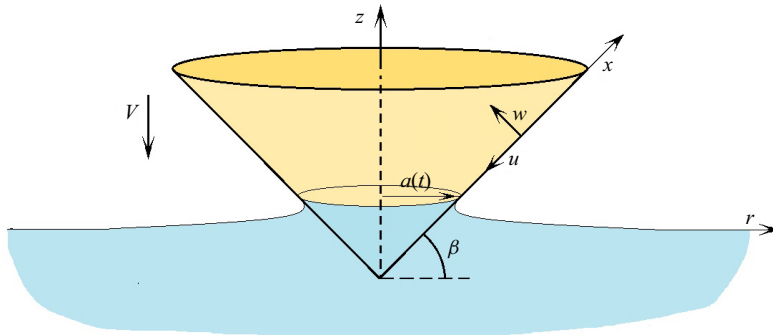


Figure 2. Sketch of an elastic cone penetrating liquid at constant speed.

deflections and strains in the cone during the impact stage, as well as hydrodynamic loads are presented and compared with the results by others in § 4. It is shown that membrane stresses might be as high as the bending stresses for some conditions of impact. The hydrodynamic pressures acting on an elastic cone can be higher than the pressures acting on the equivalent rigid cone for the same impact conditions. Finally, in § 5, the results obtained are summarised and some directions for further work are outlined.

2. Formulation of the problem

The problem of elastic shell impact onto water surface is formulated in cylindrical coordinates z, r , where z is the vertical coordinate and r is the radial coordinate, see figure 2. Initially, $t = 0$, the liquid occupies the lower half-space $z < 0$ and the position of the shell is described by the equation $z = r \tan \beta$, $r < R \cos \beta$, where β is the deadrise angle of the cone and R is the length of the cone generator (Leissa 1973), which is called length of the cone below. The shell is not stressed before impact. The tip of the shell and its edge are clamped to a rigid structure. The cone touches the flat and horizontal free surface of the liquid at a single point taken as the origin of the coordinate system.

The cone starts suddenly to penetrate the liquid vertically with a constant speed V at $t = 0$. The flow caused by the impact is assumed potential and axisymmetric. The deadrise angle of the cone β is assumed small, which makes it possible to approximate the hydrodynamic loads acting on the impacting conical shell using the Wagner approach. Gravity, surface tension and viscous effects are not taken into account in this approach (Wagner 1932). Within the Wagner approach only the early stage of the impact is considered, during which the vertical displacement of the cone is comparable with the vertical dimension of the cone, $R \sin \beta$, and is much smaller than the horizontal dimension of the wetted part of the cone, which is of the order of $R \cos \beta$. During the early stage of impact, the flow region is approximated by the lower half-space $z < 0$, the boundary conditions on the free surface, $z = \eta(r, t)$, $r > a(t)$, and on the wetted part of the deformed cone, which is approximated as $z = -Vt + r \tan \beta + w(x, t)$, $r < a(t)$, are linearised and imposed on the plane $z = 0$. Here $x = r / \cos \beta$ is the distance along the cone generator measured from the tip of the cone, $a(t)$ is the radius of the wetted part of the deformed cone during the impact stage, when $a(t) < R \cos \beta$, and $w(x, t)$ is the normal elastic displacement of the shell elements caused by the impact loads. During the next, penetration, stage, which starts when the cone is completely wetted but continues to penetrate into the liquid, we have $a(t) = R \cos \beta$. This approximation of the hydrodynamic problem of liquid impact is known also as a ‘flat-disc approximation’ because the wetted

part of the impacting surface is approximated by a flat disc, radius of which increases with time and should be determined as part of the solution.

Within the Wagner approach, the hydrodynamic pressure is given by the linearised Bernoulli equation (see Howison, Ockendon & Wilson (1991)) and the boundary-value problem for the velocity potential $\varphi(r, z, t)$ reads (see Scolan 2004)

$$\nabla^2 \varphi = 0 \quad (z < 0), \tag{2.1}$$

$$\varphi = 0 \quad (z = 0, r > a(t)), \quad \varphi_z = -V + w_t(x, t) \quad (z = 0, r < a(t)), \tag{2.2a,b}$$

$$p(r, z, t) = -\rho \varphi_t(r, z, t), \tag{2.3}$$

where ρ is the liquid density. The elastic displacements in the normal, $w(x, t)$, and tangential, $u(x, t)$, directions with respect to the initial shape of the cone, see (2), are governed by the most complete linear equations of the conical shell (see Soedel (2004) and Leissa (1973))

$$\rho_s h w_{tt} + D \nabla^4 w + \frac{12D \tan^2 \beta}{x^2 h^2} \left(w + \frac{1}{\tan \beta} [u + vxu_x] \right) = p(x, 0, t), \tag{2.4}$$

$$\rho_s h u_{tt} - K \left(u_{xx} + \frac{1}{x} u_x - \frac{1}{x^2} u \right) - \frac{K \tan \beta}{x^2} [vxw_x - w] = 0, \quad (0 < x < R), \tag{2.5}$$

$$K = \frac{12}{h^2} D, \quad D = \frac{Eh^3}{12(1 - \nu^2)}, \tag{2.6a,b}$$

with the edge

$$w = w_x = u = 0 \quad (x = 0, R), \tag{2.7}$$

and initial

$$w(x, 0) = w_t(x, 0) = u(x, 0) = u_t(x, 0) = 0, \tag{2.8}$$

conditions. Here ρ_s , E and ν are the density, Young module and Poisson ratio of the shell material and h is the shell thickness. Note that $x = r / \cos \beta \approx r$ in (2.2a,b) for small deadrise angle β . In contrast to notation in Soedel (2004) and Leissa (1973), the normal displacement $w(x, t)$ is positive upwards and the tangential displacement $u(x, t)$ is positive if a shell element is displaced towards the tip of the cone.

The problem (2.1)–(2.8) was solved by Scolan (2004) neglecting the tangential displacement $u(x, t)$ and the third term on the left-hand side of shell equation (2.4). This approximation implies that the conical shell was modelled as a circular elastic plate clamped at the edge, $x = R$, and at the centre, $x = 0$. We shall derive the conditions when this approximation by Scolan (2004) is acceptable.

The problem (2.1)–(2.8) in the dimensionless variables denoted with a tilde,

$$x = R\tilde{x}, \quad r = R\tilde{r}, \quad z = R\tilde{z}, \quad t = T_{sc}\tilde{t}, \quad w = VT_{sc}\tilde{w}(\tilde{x}, \tilde{t}), \quad u = VT_{sc} \tan \beta \tilde{u}(\tilde{x}, \tilde{t}), \tag{2.9a-f}$$

$$\varphi = VR\tilde{\varphi}(\tilde{r}, \tilde{z}, \tilde{t}), \quad p = \rho V^2 \tilde{p}(\tilde{r}, \tilde{z}, \tilde{t}) / \sin \beta, \quad a = R\tilde{a}, \quad T_{sc} = R \sin \beta / V, \tag{2.10a-d}$$

takes the form (a tilde is dropped in the following)

$$\nabla^2 \varphi = 0 \quad (z < 0), \tag{2.11}$$

$$\varphi(r, 0, t) = 0 \quad (r > a(t)), \quad \varphi_z(r, 0, t) = -1 + w_t(x, t) \quad (r < a(t)), \tag{2.12a,b}$$

$$\alpha w_{tt} + \nabla^4 w + \frac{\delta}{x^2}(w + vxu_x + u) = -\alpha\gamma\varphi_t(r, 0, t) \quad (0 < x < 1), \tag{2.13}$$

$$u_{xx} + \frac{1}{x}u_x - \frac{1}{x^2}u + \frac{1}{x^2}(vxw_x - w) = \varepsilon\alpha u_{tt} \quad (0 < x < 1), \tag{2.14}$$

$$w = w_x = u = 0 \quad (x = 0, 1), \quad w = w_t = u = u_t = 0 \quad (t = 0). \tag{2.15a,b}$$

The dimensionless parameters in (2.13) and (2.14) are

$$\alpha = 12(1 - \nu^2) \left(\frac{VR}{c_p h \sin \beta} \right)^2, \quad \gamma = \frac{\rho R}{\rho_s h}, \quad \delta = 12 \tan^2 \beta \frac{R^2}{h^2}, \quad \varepsilon = \frac{1}{12} \left(\frac{h}{R} \right)^2, \tag{2.16a-d}$$

where $c_p = \sqrt{E/\rho_s}$, is known as the speed of pressure waves in a shell material.

We assume that the impact conditions are such that $\alpha = O(1)$. For shells, we have $\varepsilon \ll 1$ and $\gamma < 1$. As to the parameter δ , we have $\tan \beta \ll 1$ within the Wagner model of water impact, and $R/h \gg 1$ for thin-walled shells, with their product being large or small depending on the characteristics of the cone. Therefore, we can neglect the term $\varepsilon\alpha u_{tt}$ in (2.14), as it was done by Grigolyuk & Gorshkov (1971), but should keep the term with δ . In the study by Scolan (2004), the term with δ was neglected for the parameters $R = 0.128$ m, the deadrise angle β in the range from 6° to 20° , and the shell thickness h being from 0.5 to 15 mm. The minimum value of δ for these parameters is 8.7 which is achieved for the most stiff shell with $h = 15$ mm and $\beta = 6^\circ$. The maximum value $\delta = 101\,921$ is achieved for $h = 0.5$ mm and $\beta = 20^\circ$.

For the parameters used by Malenica *et al.* (2022), $E = 2.1 \times 10^{11}$ Pa, $\rho_s = 7850$ kg m⁻³, $h = 0.01$ m, $R = 1$ m, $\beta = 10^\circ$, and $\nu = 0.3$, $\rho = 1000$ kg m⁻³ and $V = 2$ m s⁻¹, we have $\delta = 3730.9445$, $\varepsilon = 8.33 \times 10^{-6}$, $c_p = 5172.2$ m s⁻¹, $\gamma = 12.74$, $\alpha = 0.5412$ and $\alpha\gamma = 6.895$. We conclude that the parameter δ is not small for small deadrise angles and, therefore, the term with δ in (2.13) should be retained.

Equation (2.14), where the right-hand side is approximated by zero for small ε , can be integrated with account for the edge conditions $u(0, t) = u(1, t) = 0$ with the result

$$u(x, t) = Cx + \frac{1 - \nu}{2}x \int_0^x w(x_0, t) \frac{dx_0}{x_0^2} - \frac{1 + \nu}{2x} \int_0^x w(x_0, t) dx_0, \tag{2.17}$$

$$C = -\frac{1 - \nu}{2} \int_0^1 w(x_0, t) \frac{dx_0}{x_0^2} + \frac{1 + \nu}{2} \int_0^1 w(x_0, t) dx_0. \tag{2.18}$$

The physical strains on the inner and outer surfaces of the conical shell are given by

$$\varepsilon_{xx}(x, t) = \varepsilon_{sc} \left(\sqrt{\frac{\delta}{3}} \frac{\partial u}{\partial x} \mp \frac{\partial^2 w}{\partial x^2} \right), \quad \varepsilon_{\theta\theta}(x, t) = \varepsilon_{sc} \frac{1}{x} \left(\sqrt{\frac{\delta}{3}}(u + w) \mp \frac{\partial w}{\partial x} \right), \tag{2.19a,b}$$

where $u(x, t)$, $w(x, t)$ and x are dimensionless variables, and $\varepsilon_{sc} = h \sin \beta / (2R)$. Here $\varepsilon_{xx}(x, t)$ is the relative elongation of a shell element along the cone generator, $\varepsilon_{\theta\theta}(x, t)$ is the relative elongation of a shell element in the angular azimuthal direction, see figure 3,

Water entry of an elastic conical shell

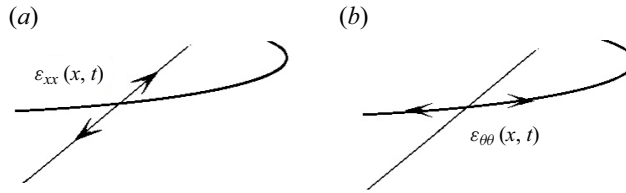


Figure 3. Sketch of radial (a) and azimuthal (b) strains.

minus/plus in (2.19a,b) stand for the inner/outer surface of the shell. The strains can be decomposed also as

$$\varepsilon_{xx}(x, t) = \varepsilon_{xx}^{(m)}(x, t) \mp \varepsilon_{xx}^{(b)}(x, t), \quad \varepsilon_{\theta\theta}(x, t) = \varepsilon_{\theta\theta}^{(m)}(x, t) \mp \varepsilon_{\theta\theta}^{(b)}(x, t), \quad (2.20a,b)$$

where the superscript (*m*) stands for membrane strains and the superscript (*b*) for bending strains (see Soedel 2004).

We are searching the solution of the hydrodynamic problem (2.1)–(2.3) with square-root singularity of the flow velocity and the pressure at the contact line, where the boundary conditions (2.2a,b) change their type (see Howison *et al.* (1991), Scolan & Korobkin (2001) and Scolan (2004)). The flow is not singular at the tip of the cone, $x = 0$, but the strains are singular there. The displacements of the conical shell should be such that the potential energy of the deformed shell is finite during the cone entry into the liquid. This condition provides $w(x, t) = O(x^2 \log x)$ as $x \rightarrow 0$. Note that $\nabla^2(x^2 \log x) = 0$. Therefore, the strains $\varepsilon_{xx}(x, t)$ and $\varepsilon_{\theta\theta}$ are of order $O(\log x)$ as $x \rightarrow 0$.

3. Solution by the normal mode method

The coupled problem of hydroelasticity (2.1)–(2.16a–d) can be solved using the dry modes of the conical shell. A dry mode consists of normal and tangential displacements of the shell elements. Then (2.13) with account for (2.17) and (2.18) can be reduced to simple harmonic oscillator equations for the amplitude of each dry mode with their right-hand sides being projections of the hydrodynamic loads onto the modes. In the present approach, the tangential displacement $u(x, t)$ is related to the normal displacement $w(x, t)$ by (2.17) and (2.18). These relations together with (2.13) provide an integro-differential equation for the function $w(x, t)$ which is solved by using the modes introduced by Scolan (2004), which are the dry modes of a circular elastic plate clamped at the centre and at the edge. These dry modes correspond to the shell equation (2.13), where $\delta = 0$ and $\gamma = 0$. The same idea is expected to be practical in the hydroelastic slamming problems for complex structures, where normal modes of an elastic plate with the same edge conditions and internal supports are used instead of the modes of the actual structure. This idea was used by Korobkin, Khabakhpasheva & Shishmarev (2023) to determine wet modes and the corresponding added-mass matrices for complex two-dimensional elastic structures in contact with liquid.

The Scolan's modes, $\psi_n(r)$, are solutions of the eigenvalue problem,

$$\nabla^4 \psi_n = \lambda_n^4 \psi_n \quad (0 < r < 1), \quad \psi_n = \psi_n' = 0 \quad (r = 0, 1), \quad (3.1a,b)$$

where λ_n are the corresponding eigenvalues, $0 < \lambda_n < \lambda_{n+1}$ and $n \geq 1$. The modes are orthogonal,

$$\int_0^1 \psi_n(r) \psi_m(r) r \, dr = \delta_{nm}, \quad (3.2)$$

and have the form

$$\psi_n(r) = A_n \left\{ C_n [J_0(\lambda_n r) - I_0(\lambda_n r)] - Y_0(\lambda_n r) - \frac{2}{\pi} K_0(\lambda_n r) \right\} \quad (3.3)$$

$$C_n = \frac{Y_0(\lambda_n) + (2/\pi)K_0(\lambda_n)}{J_0(\lambda_n) - I_0(\lambda_n)}, \quad (3.4)$$

see Scolan (2004) for the details and the dispersion relation for the eigenvalues λ_n . Here $\delta_{nn} = 1$ and $\delta_{nm} = 0$ for $n \neq m$. The coefficients A_n are determined numerically using the condition (3.2) for $m = n$. The modes behave as $\psi_n(r) \sim (A_n \lambda_n^2 / \pi) r^2 \log r$ for $r \rightarrow 0$, which corresponds to the expected behaviour of the normal deflection near the tip of the cone, see Leissa (1973).

The normal deflection of the conical shell and the velocity potential are sought in the form of the series,

$$w(r, t) = \sum_{n=1}^{\infty} b_n(t) \psi_n(r), \quad (3.5)$$

$$\varphi(r, z, t) = \varphi_0(r, z, a) + \sum_{n=1}^{\infty} \dot{b}_n(t) \varphi_n(r, z, a), \quad (3.6)$$

where the potentials $\varphi_n(r, z, a)$ are the solutions of the boundary problem (2.1)–(2.2a,b) with the condition on the wetted part of the cone, where $r < a(t)$, being replaced by $\varphi_{0z}(r, 0, a) = -1$ and $\varphi_{nz}(r, 0, a) = \psi_n(r)$ for $n \geq 1$. The potential $\varphi_0(r, z, a)$ is the potential of the flow caused by entry of the rigid cone into the liquid half-space. The potentials $\varphi_n(r, z, a)$ are independent of time at the penetration stage, when the cone is completely wetted, $a(t) = 1$, but continues to penetrate the liquid at the constant speed vibrating elastically.

3.1. Impact stage

It is convenient to introduce a function

$$q(r, t) = w_t(r, t) + \gamma \varphi(r, 0, t) \quad (r < a(t)), \quad q(r, t) = w_t(r, t) \quad (a(t) < r < 1), \quad (3.7a,b)$$

and present it, in the interval $0 < r < 1$, by the series

$$q(r, t) = \sum_{n=1}^{\infty} q_n(t) \psi_n(r). \quad (3.8)$$

Equations (3.5), (3.7a,b) and the orthogonality condition (3.2) provide the coefficients $q_n(t)$,

$$q_n = \frac{db_n}{dt} + \gamma \sum_{m=1}^{\infty} \frac{db_m}{dt} S_{mn}(a) + \gamma f_n(a), \quad (3.9)$$

$$f_n(a) = \int_0^a \varphi_0(r, 0, a) \psi_n(r) r dr, \quad S_{mn}(a) = \int_0^a \varphi_m(r, 0, a) \psi_n(r) r dr. \quad (3.10a,b)$$

The symmetric matrix $\mathbb{S}(a)$ with the elements $S_{nm}(a)$ given by (3.10a,b) is known as the added-mass matrix of a circular elastic plate of radius 1, which is in contact with the liquid

only over the region $r < a$. This matrix was derived by Scolan (2004). The solution of the hydrodynamic problem,

$$\nabla^2 \varphi_n = 0 \quad (z < 0), \quad \varphi_n = 0 \quad (z = 0, r > a), \quad \varphi_{nz} = \psi_n(r) \quad (z = 0, r < a), \tag{3.11a-c}$$

where $n \geq 0$ and $\psi_0(r) = -1$, reads

$$\varphi_n(r, 0, a) = a \int_r^a \frac{\chi_n(\xi/a) d\xi}{\sqrt{\xi^2 - r^2}}, \quad \chi_n(\mu) = \frac{2}{\pi} \int_0^\mu \frac{\sigma \psi_n(a\sigma) d\sigma}{\sqrt{\mu^2 - \sigma^2}}. \tag{3.12a,b}$$

The solution (3.12a,b) is convenient to present as

$$\left. \begin{aligned} \chi_n(\mu) &= \frac{2}{\pi} \mu Q_n(a\mu), \quad \varphi_n(r, 0, a) = \frac{2}{\pi} \int_r^a \frac{\xi Q_n(\xi) d\xi}{\sqrt{\xi^2 - r^2}}, \\ Q_n(\xi) &= \int_0^{\pi/2} \psi_n(\xi \sin \theta) \sin \theta d\theta. \end{aligned} \right\} \tag{3.13}$$

Then it is easy to show that

$$Q_0(\xi) = -1, \quad \varphi_0(r, 0, a) = -\frac{2}{\pi} \sqrt{a^2 - r^2}, \tag{3.14a,b}$$

where $0 < r < a$, and

$$S_{nm}(a) = \frac{2}{\pi} \int_0^a x^2 Q_n(x) Q_m(x) dx. \tag{3.15}$$

The functions $Q_n(a)$ and $S_{nm}(a)$ are oscillating in the interval $0 \leq a \leq 1$. The calculations revealed that the derivative $Q'_n(a)$ changes its sign n times in this interval. In each subinterval, where $Q'_n(a)$ has a certain sign, the function $Q_n(a)$ can be approximately presented by 25 points. In total, the function $Q_n(a)$ is presented by $25n$ points with distance $1/(25n)$ between the points. The derivatives of the added-mass elements, $S'_{nm}(a) = (2/\pi)a^2 Q_n(a) Q_m(a)$, and $S_{nm}(a)$ as well, are also oscillating. The elements $S_{nm}(a)$ for $m \leq n$ can be approximately presented with $25n$ points, which are the same as for $Q_n(a)$. Between these points, the functions $Q_n(a)$ and $S_{nm}(a)$ are approximated linearly. By using this approximations, the functions $Q_n(a)$ and $S_{nm}(a)$ are precalculated numerically for a from zero to one with step 0.002 for $1 \leq n \leq m \leq 20$. The added-mass matrix is constant $\mathbb{S}(1)$ at the penetration stage, when the elastic cone is completely wetted.

Equation (2.13) for the normal displacement $w(r, t)$ of the shell elements can be written now as

$$\frac{\partial q}{\partial t} = -\frac{1}{\alpha} \left\{ \nabla^4 w + \frac{\delta}{r^2} (w + vru_r + u) \right\}. \tag{3.16}$$

Substituting (3.8), (3.5), (2.17) and (2.18) into (3.16), multiplying both sides of the equation by $r\psi_m(r)$, and integrating the result with respect to r from $r = 0$ to $r = 1$ with account

for (3.1a,b), we obtain

$$\frac{dq_m}{dt} = -\frac{1}{\alpha} \left\{ \lambda_m^4 b_m + \delta \sum_{n=1}^{\infty} b_n(t) T_{mn} \right\}, \quad (3.17)$$

where

$$T_{mn} = \frac{1}{2}(1 + \nu)^2 \int_0^1 \psi_n(r) dr \int_0^1 \psi_m(r) dr + (1 - \nu^2) \left\{ \int_0^1 \psi_m(r) \psi_n(r) \frac{dr}{r} - \frac{1}{2} \int_0^1 \psi_m(r) \int_0^r \psi_n(r_0) dr_0 \frac{dr}{r^2} - \frac{1}{2} \int_0^1 \psi_n(r) \int_0^r \psi_m(r_0) dr_0 \frac{dr}{r^2} \right\}. \quad (3.18)$$

The matrix \mathbb{T} with the elements T_{nm} given by (3.18) is symmetric and depends only on the Poisson ratio ν of the shell material. This matrix is precalculated numerically using the orthonormal functions (3.3).

Equations (3.9) and (3.17) and the initial conditions (2.8) can be written in the matrix form,

$$\left. \begin{aligned} \frac{d\mathbf{b}}{dt} &= (\mathbb{I} + \gamma \mathbb{S}(a))^{-1} (\mathbf{q} - \gamma \mathbf{f}(a)) & \frac{d\mathbf{q}}{dt} &= -\frac{1}{\alpha} (\mathbb{D} + \delta \mathbb{T}) \mathbf{b}, \\ \mathbf{b}(0) &= 0, & \mathbf{q}(0) &= 0, \end{aligned} \right\} \quad (3.19)$$

where $\mathbb{D} = \text{diag}(\lambda_1^4, \lambda_2^4, \lambda_3^4, \dots)$ is a diagonal matrix, $\mathbf{b}(t) = (b_1, b_2, b_3, \dots)^T$, $\mathbf{q}(t) = (q_1, q_2, q_3, \dots)^T$ and $\mathbf{f}(a) = (f_1, f_2, f_3, \dots)^T$.

The radius $a(t)$ of the wetted part of the cone during the impact stage is calculated using the Wagner condition that the elevation of the liquid free surface is equal to the vertical coordinate of the deformed surface of the cone at $r = a(t)$. This condition was reduced by Scolan (2004) to the equation, which in the dimensionless variables (2.10a–d) has the form

$$a(t) = \frac{4}{\pi} \left(t - \sum_{n=1}^{\infty} b_n(t) Q_n(a) \right). \quad (3.20)$$

The system (3.19) and (3.20) is integrated in time up to a time instant t_* , when $a(t_*) = 1$. Note that the dimensionless duration of the impact stage for a rigid cone is equal to $\pi/4$. Indeed, for a rigid cone, we should set $b_n = 0$ in (3.20), which gives $a(t) = 4t/\pi$ and $a = 1$ at $t = \pi/4$.

3.2. Penetration stage and wet/dry modes

For $t > t_*$, when the shell is completely wetted but continues to penetrate into the liquid, we set $a = 1$, $\mathbf{f} = \mathbf{f}(1)$, $\mathbb{S} = \mathbb{S}(1)$ and continue numerical integration of the system (2.3) in time using the matching conditions,

$$\mathbf{b}(t_* + 0) = \mathbf{b}(t_* - 0), \quad \mathbf{q}(t_* + 0) = \mathbf{q}(t_* - 0), \quad (3.21a,b)$$

where $\mathbf{b}(t_* - 0)$ and $\mathbf{q}(t_* - 0)$ are the solutions of the initial problem (3.19) at the end of the impact stage.

It is convenient to introduce a new unknown vector $\mathbf{g}(t) = \mathbf{q}(t) - \gamma \mathbf{f}(1)$. Then the system (3.19) at the penetration stage and the matching conditions (3.21a,b) read

$$\left. \begin{aligned} \frac{d\mathbf{b}}{dt} &= (\mathbb{I} + \gamma \mathbb{S}(1))^{-1} \mathbf{g}, & \frac{d\mathbf{g}}{dt} &= -\frac{1}{\alpha} (\mathbb{D} + \delta \mathbb{T}) \mathbf{b}, \\ \mathbf{b}(t_* + 0) &= \mathbf{b}(t_* - 0), & \mathbf{g}(t_* + 0) &= \mathbf{q}(t_* - 0) - \gamma \mathbf{f}(1). \end{aligned} \right\} \quad (3.22)$$

The homogeneous system (3.22) of ordinary differential equations without the matching conditions at $t = t_*$ has a periodic solution $\mathbf{b}(t) = \mathbf{B} \cos(\Omega t)$, where the constant vector \mathbf{B} is a solution of the system

$$((\mathbb{I} + \gamma \mathbb{S}(1))^{-1} (\mathbb{D} + \delta \mathbb{T}) - \mu \mathbb{I}) \mathbf{B} = 0. \quad (3.23)$$

Non-zero solutions of the system (3.23) with symmetric matrix $(\mathbb{I} + \gamma \mathbb{S}(1))^{-1} (\mathbb{D} + \delta \mathbb{T})$ exist only if $\mu = \alpha \Omega^2$ is an eigenvalue of this matrix. The eigenvalues are numbered in such a way that $\mu_n^{(w)} < \mu_{n+1}^{(w)}$ where $n \geq 1$ and the superscript w stands for wet conditions. The eigenvalues depend on parameters γ and δ and are independent of the shell rigidity and speed of the impact. The corresponding solutions $\mathbf{B}_n^{(w)}$ of the system (3.23) for $\mu = \mu_n^{(w)}$ provide the so-called wet modes,

$$W_n^{(w)}(r) = \sum_{j=1}^{\infty} B_{nj}^{(w)} \psi_j(r), \quad (3.24)$$

of the completely wetted conical shell. Note that the determinant of the matrix of system (3.23) at $\mu = \mu_n^{(w)}$ is zero. To find the vector $\mathbf{B}_n^{(w)}$, we truncate the system retaining $(N_{mod} - 1)$ equation and setting $B_{n,j}^{(w)} = 0$ for $j > N_{mod}$ and $B_{n,N_{mod}}^{(w)} = 1$. Finally, the vector $\mathbf{B}_n^{(w)}$ is rescaled in such a way that $B_{n,n}^{(w)} = 1$. The wet modes $W_n^{(w)}(r)$ are orthogonal but not orthonormal,

$$\int_0^1 W_n^{(w)}(r) W_m^{(w)}(r) r \, dr = \eta_n^2 \delta_{nm}, \quad (3.25)$$

where $\eta_n^2 = (\mathbf{B}_n^{(w)} \mathbf{B}_n^{(w)})$. The wet modes of partially wetted cone are different from the modes of the totally wetted cone and are not considered in the present analysis.

The dimensionless angular frequency $\Omega_n^{(w)}$ of the wet n th mode $W_n^{(w)}(r)$ is equal to $\Omega_n^{(w)} = (\mu_n^{(w)} / \alpha)^{1/2}$. The corresponding dimensional angular frequency of the n th wet mode is equal to $\omega_n^{(w)} = \Omega_n^{(w)} / T_{sc} = (\mu_n^{(w)} / \alpha)^{1/2} / T_{sc} = [\mu_n^{(w)} D / (\rho_s h R^4)]^{1/2}$. The ratio of the duration of the impact stage $T_{(im)}$, which is equal to $\pi / 4 T_{sc}$ for constant impact speed and rigid cone, to the period of the first wet mode, $T_1^{(w)} = 2\pi / \omega_1^{(w)}$, is equal to

$$\frac{T_{(im)}}{T_1^{(w)}} = \frac{1}{8} \Omega_1^{(w)} = \frac{1}{8} \sqrt{\frac{\mu_1^{(w)}}{\alpha}}. \quad (3.26)$$

This ratio is inverse proportional to the impact speed V , see the definition of the parameter α in (2.16a–d). The smallest eigenvalue $\mu_1^{(w)}$ of the matrix in (3.23), which appears in (3.26), depends on the deadrise angle β , length of the cone R and thickness h of the shell through the parameter δ and on the density of the shell material ρ_s and the density of the liquid ρ through the parameter γ and is independent of the shell rigidity.

The time ratio (3.26) is used to identify the regime of the hydroelastic impact (see Faltinsen (1999, 2000) and Malenica *et al.* (2021, 2022)). If the ratio is large, this is the impact duration is much longer than the period of the lowest wet mode, then the elastic behaviour of an elastic structure during water impact is well described by the so-called quasi-static decoupled approximation. Within this approximation, one calculates the hydrodynamic pressures acting on an equivalent rigid cone and then applies these pressures to the elastic structure without account for the structural inertia, see § 1.1. For small time ratio (3.26), see figure 1, the impact duration $T_{(im)}$ is short and the maximum deflections and stresses occur at the penetration stage, where the lowest wet modes $W_n^{(w)}(r)$ provide main contributions, see Korobkin & Khabakhpasheva (2006).

By using the wet modes $W_n^{(w)}(r)$, the equations (3.22) can be explicitly integrated. During the penetration stage, the deflection of the conical shell can be presented as the series with respect to wet modes:

$$w(r, t) = \sum_{n=1}^{\infty} C_n(t) W_n^{(w)}(r), \tag{3.27}$$

instead of the series (3.5), which is with respect to the simplified modes. The coefficients $C_n(t)$ are related to the coefficients $b_n(t)$ in (3.5) by

$$\mathbf{b} = \mathbb{B}^{(w)} \mathbf{C}, \tag{3.28}$$

where $\mathbf{C}(t) = (C_1, C_2, C_3, \dots)^T$ and the columns of the matrix $\mathbb{B}^{(w)}$ are the vectors $\mathbf{B}_n^{(w)}$. Then the system (3.22) leads to the following equations for the coefficients $C_n(t)$, $n \leq 1$,

$$\frac{d^2 C_n}{dt^2} + (\Omega_n \eta_n)^2 C_n = 0 \quad (t > t_*). \tag{3.29}$$

The matching conditions (3.21a,b) provide

$$C_n(t_* + 0) = (\mathbb{B}^{(w)})^T \mathbf{b}(t_* - 0), \tag{3.30}$$

$$\frac{dC_n}{dt}(t_* + 0) = (\mathbb{B}^{(w)})^T (\mathbb{I} + \gamma \mathbb{S}(1))^{-1} \mathbf{g}(t_* - 0). \tag{3.31}$$

Therefore, the formulae, $n \geq 1$,

$$C_n(t) = C_n(t_* + 0) \cos[\Omega_n \eta_n(t - t_*)] + \frac{dC_n}{dt}(t_* + 0) \frac{1}{\Omega_n \eta_n} \sin[\Omega_n \eta_n(t - t_*)], \tag{3.32}$$

yield explicit solution of the initial problem (3.29)–(3.31) for the penetration stage.

If the elastic cone is not in contact with water, then its natural oscillations are also described by the system (3.23) but now with $\gamma = 0$. The corresponding eigenvalues $\mu_n^{(d)}$ and solutions $\mathbf{B}_n^{(d)}$ are denoted with superscript (d) and calculated in the same way as for the wet modes. The corresponding dimensional angular frequency of the n th dry mode is equal to $\omega_n^{(d)} = \Omega_n^{(d)} / T_{sc} = (\mu_n^{(d)} / \alpha)^{1/2} / T_{sc} = [\mu_n^{(d)} D / (\rho_s h R^4)]^{1/2}$, where $\mu_n^{(d)}$ depends only on the parameter δ . Note that the ratios $\omega_n^{(w)} / \omega_n^{(d)}$ are independent of the shell rigidity.

The dry modes of an elastic conical shell are not used in the present algorithm. They are calculated together with the corresponding natural frequencies as part of the numerical solution of the hydroelastic fully nonlinear slamming problems (see Malenica *et al.* 2022) within the modal approach. In this approach the displacements of an elastic shell are sought as a combination of the dry modes of the shell with unknown

time-dependent coefficients. The matrix equation of structural dynamics with respect to these coefficients is much simpler than the original finite-element equation. This matrix equation is solved together with the discretised equations of computational fluid dynamics using an iterative algorithm with an under-relaxation scheme. It is known that iterations do not converge without such a scheme for hydroelastic problems with a strong added-mass effect (see Seng, Jensen & Malenica (2014) and Causin, Gerbeau & Nobile (2005)). One of the options for numerical solving of hydroelastic slamming problem is to ‘... subtract an added mass force from both sides of the [structural] equation... Then the [structural] acceleration is obtained by dividing the resulting force by the sum of a [structural] mass and a first approximation of the added-mass [matrix]’, see the ‘Fluid–structure coupled analysis’ in Sun & Faltinsen (2006). We suggest to use the added-mass matrix calculated within the Wagner model of hydroelastic slamming as the ‘first approximation of the added-mass matrix’ mentioned by Sun & Faltinsen (2006). This added-mass matrix for dry modes of the structure can be obtained using the added-mass (3.15) for simplified structure and the solutions $\mathbf{B}_n^{(d)}$, $\mu_n^{(d)}$ of the system (3.23) for $\gamma = 0$. Such a combination of numerical and analytical approaches is under investigation at present.

3.3. Hydrodynamic loads

The present approach, where the system (3.19) is integrated in time during the impact stage with $a(t) < 1$ and the system (3.22) is integrated in time during the penetration stage with $a(t) = 1$, does not require explicit evaluation of the hydrodynamic loads. The loads are difficult to compute and measure in problems of hydrodynamic slamming (see Faltinsen (1999, 2000) and Malenica *et al.* (2022)). The pressure $p(x, 0, t)$ can be reconstructed from the equation for the normal displacements of the shell elements (2.13). In the dimensionless variables (2.10a–d), we have $p(r, 0, t) = -\varphi_t(r, 0, t)$. Substituting the series for the normal displacements (3.5) into the dimensionless shell equation (2.13), and using (3.7a,b) and (3.16), we find

$$p(r, 0, t) = \sum_{n=1}^{\infty} p_n(t)\psi_n(r), \tag{3.33}$$

$$p_n(t) = \frac{1}{\gamma} \frac{d^2 b_n}{dt^2} + \frac{1}{\alpha\gamma} \left\{ \lambda_n^4 b_n + \delta \sum_{m=1}^{\infty} b_m(t) T_{nm} \right\}. \tag{3.34}$$

Note that $0 < r < 1$ in (3.33), and $p(r, 0, t) = 0$, where $a(t) < r < 1$ during the impact stage. The second derivatives $d^2 b_n/dt^2$ in (3.33) are calculated for the impact stage using the system

$$(\mathbb{I} + \gamma\mathbb{S}(a)) \frac{d^2 \mathbf{b}}{dt^2} = \frac{d\mathbf{q}}{dt} + \gamma \frac{da}{dt} \left\{ \frac{2a^2}{\pi} \mathbf{Q} - \mathbb{S}'(a) \frac{d\mathbf{b}}{dt} \right\}, \tag{3.35}$$

which is obtained by differentiation (3.19) with respect to time. Here $da/dt = 0$ at the penetration stage. Note that (3.10a,b), (3.13) and (3.14a,b) give

$$f'_n(a) = -\frac{2a^2}{\pi} Q_n(a). \tag{3.36}$$

In (3.35), the derivatives $d\mathbf{b}/dt$ and $d\mathbf{q}/dt$ are calculated using (3.19), the derivative da/dt is obtained by differentiation (3.20) with respect to time,

$$\frac{da}{dt} = \frac{1 - Q(a) \cdot db/dt}{\pi/4 + Q'(a) \cdot b}, \tag{3.37}$$

where $Q(a) = (Q_1(a), Q_2(a), Q_3(a), \dots)^T$, $Q'(a) = (Q'_1(a), Q'_2(a), Q'_3(a), \dots)^T$ and $Q_n(a)$ are given by (3.13), and

$$Q'_n(\xi) = \int_0^{\pi/2} \psi'_n(\xi \sin \theta) \sin^2 \theta \, d\theta, \quad S'_{nm}(a) = \frac{2}{\pi} a^2 Q_n(a) Q_m(a). \tag{3.38a,b}$$

On the other hand, the linearised Bernoulli equation, $p(r, 0, t) = -\varphi_t(r, 0, t)$, the series (3.5) for the velocity potential, and the formulae (3.13), (3.14a,b) and (3.37) provide

$$p(r, 0, t) = \frac{B(t)}{\sqrt{a^2 - r^2}} - \sum_{n=1}^{\infty} \frac{d^2 b_n}{dt^2} \varphi_n(r, 0, a), \tag{3.39}$$

$$B(t) = \frac{2}{\pi} a \dot{a} \left(1 - \sum_{n=1}^{\infty} \frac{db_n}{dt} Q_n(a) \right). \tag{3.40}$$

Equations (3.13) yield that $\varphi_n(r, 0, t) = O(\sqrt{a^2 - r^2})$ as $r \rightarrow a$ and $r < a$. We conclude that the pressure is square-root singular at the contact line $r = a(t)$ during the impact stage, $p(r, 0, t) = O(1/\sqrt{a^2 - r^2})$, and behaves as $p(r, 0, t) = O(\sqrt{1 - r^2})$ during the penetration stage, where $r \rightarrow 1 - 0$. As a result, the series (3.33) converges slowly when $a(t) < 1$. To improve the convergence, we decompose the series (3.33) during the impact stage as

$$p(r, 0, t) = B(t) \frac{H(a^2 - r^2)}{\sqrt{a^2 - r^2}} + \sum_{n=1}^{\infty} \tilde{p}_n(t) \psi_n(r), \tag{3.41}$$

where $H(x)$ is the Heaviside step function, $H(x) = 1$ for $x \geq 0$ and $H(x) = 0$ for $x < 0$. Multiplying both sides of (3.41) by $\psi_m(r)r$ and integrating the results with respect to r from zero to one using the orthogonality relation (3.2), we find

$$\tilde{p}_m(t) = p_m(t) - aB(t)Q_m(a), \tag{3.42}$$

during the impact stage where $a(t) < 1$. During the penetration stage, we have $a(t) = 1$ and $B(t) = 0$ in (3.42). Coefficients \tilde{p}_m decay quicker as $m \rightarrow \infty$ than $p_m(t)$ given by (3.33).

Note that the pressure in the problem of rigid cone impact reads

$$p^{(R)}(r, 0, t) = \frac{8a}{\pi^2} \frac{H(a^2 - r^2)}{\sqrt{a^2 - r^2}}. \tag{3.43}$$

The dimensionless hydrodynamic force $F(t)$ acting on the entering elastic cone is obtained using (3.41), as

$$F(t) = 2\pi \int_0^{a(t)} p(r, 0, t)r \, dr = 2\pi aB(t)H(1 - a) + 2\pi \sum_{n=1}^{\infty} \tilde{p}_n(t) \int_0^{a(t)} \psi_n(r)r \, dr, \tag{3.44}$$

where the scale of the force is $\rho V^2 R^2$.

4. Numerical results

Calculations are performed for two cases. In case 1, which was considered by Scolan (2004), a conical shell was made of aluminium with density $\rho_s = 2700 \text{ kg m}^{-3}$, Young modulus $E = 1.2 \times 10^{11} \text{ N m}^{-2}$ and Poisson ratio $\nu = 0.3$. The thickness of the shell $h = 1.5 \text{ mm}$, the length of the cone (the length of the generator segment) is $R = 12.8 \text{ cm}$, and deadrise angle 6° . The conical shell entered water at constant speed 8.28 m s^{-1} , which corresponds to a free drop test from the height 3.5 m . We shall compare the results of the present model in the terms of the structural deflection and radius of the contact region with those predicted by the Scolan model, which corresponds to the present model with $\delta = 0$. Note that, in the conditions of case 1, $\delta = 965.3$. The deadrise angle of 6° is visually small and it looks reasonable to approximate the cone with such small deadrise angle by a circular plate. The present analysis with equations of conical shells demonstrates that this approximation is too rough. Scolan (2004) did not study dry and wet modes of a conical shell. His results are for the deflection of the circular plate, the radius of its wetted part, and impact pressure.

Case 2, which was considered by Malenica *et al.* (2022), a conical shell was made of steel with density $\rho_s = 7850 \text{ kg m}^{-3}$, Young modulus $E = 2.1 \times 10^{11} \text{ N m}^{-2}$ and Poisson ratio $\nu = 0.3$. The thickness of the shell $h = 1 \text{ cm}$, the length of the cone is $R = 1 \text{ m}$ and deadrise angle 10° . The constant entry speed was varied from 1 to 16 m s^{-1} . The dimensionless parameters in this case are $\delta = 3730.9$ and $\gamma = 12.74$. This case was selected by Malenica *et al.* (2022) to determine the DAF for an elastic cone. We shall compare the dry frequencies of the conical shell, computed by Malenica *et al.* (2022) with the frequencies predicted by the present model. Note that computations of the structural deflections were performed Malenica *et al.* (2022) not for an elastic cone, but for a fictitious structure, dry modes of which are the modes of the corresponding elastic circular plate obtained by Scolan (2004).

The ratio of the wetting time, which is estimated as $T_{(im)} = (\pi R \sin \beta)/(4V)$, and the period of the first fully wetted mode $T_1^{(w)}$, see (3.26), is equal to 0.558 for case 1. In case 2, this ratio is equal to 1.13 for speed $V = 12 \text{ m s}^{-1}$ and 2.26 for speed $V = 6 \text{ m s}^{-1}$. This ratio is important for identifying regime of hydroelastic interactions, see Malenica *et al.* (2022). Then case 1 corresponds to the impulsive regime, case 2 with $V = 12 \text{ m s}^{-1}$ to the dynamic regime and case 2 with $V = 6 \text{ m s}^{-1}$ to the quasi-static regime.

4.1. Wet/dry modes and their frequencies

The angular frequencies of the wet, $\omega^{(w)}$, and dry, $\omega^{(d)}$, modes of elastic conical shell are obtained using the roots μ_n , where $\mu_{n+1} > \mu_n$ and $n \geq 1$, of the equation,

$$\det((\mathbb{I} + \gamma \mathbb{S}(1))^{-1}(\mathbb{D} + \delta \mathbb{T}) - \mu \mathbb{I}) = 0, \tag{4.1}$$

with $\gamma > 0$ and $\gamma = 0$ correspondingly for the conditions of case 2. The dry, $\omega_n^{(d)}/2\pi$, and wet $\omega_n^{(w)}/2\pi$, frequencies as functions of the cone deadrise angle β are shown in figure 4(a) and 4(b). To calculate four lowest frequencies, the matrix $((\mathbb{I} + \gamma \mathbb{S}(1))^{-1}(\mathbb{D} + \delta \mathbb{T}) - \mu \mathbb{I})$ is truncated retaining 20 terms and its determinant is calculated as a function of μ with a certain step starting from $\mu = 0$. The intervals, where the determinant changes its sign, are identified and the bisection method is used within each interval to find the roots μ_n with a required accuracy of 10^{-10} .

The ratios of the corresponding wet and dry frequencies, see figure 4(c), weakly depend on the cone deadrise angle. The mean values $\Delta w_n^{(av)}$ of the ratios in the interval

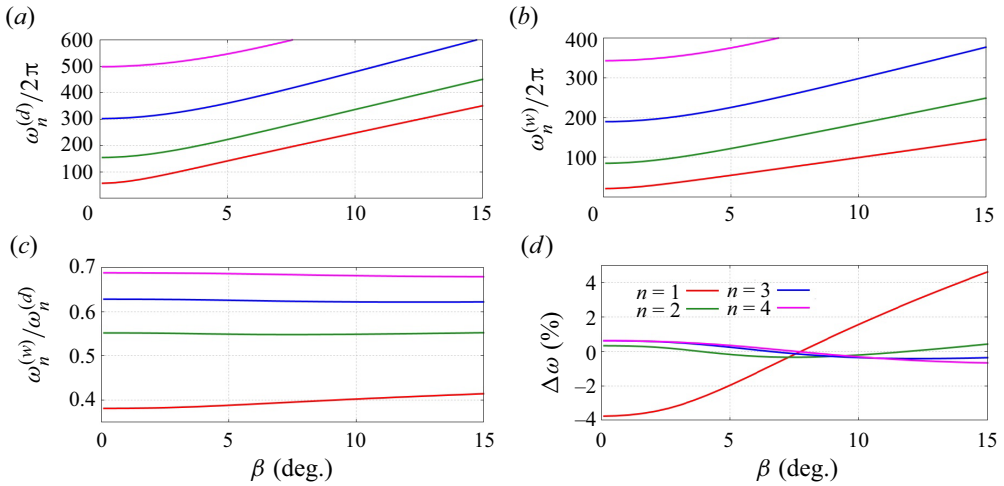


Figure 4. The frequencies of dry (a) and wet (b) modes with $n = 1, 2, 3, 4$ as functions of the cone deadrise angle β for case 2. The ratios of wet and dry frequencies for lowest modes with $n = 1, 2, 3, 4$ (c) and the deviations of the ratios from their mean values (d) in percentage.

$0 \leq \beta \leq 15^\circ$ are $\Delta\omega_1^{(av)} = 0.396$, $\Delta\omega_2^{(av)} = 0.55$, $\Delta\omega_3^{(av)} = 0.624$ and $\Delta\omega_4^{(av)} = 0.683$. The relative deviations of the ratios from their mean values,

$$\Delta\omega_n = \frac{\omega_n^{(w)}(\beta)/\omega_n^{(d)}(\beta) - \Delta\omega_n^{(av)}}{\Delta\omega_n^{(av)}} \cdot 100\%, \quad (4.2)$$

are shown in figure 4(d) for $n = 1, 2, 3$ and 4. We conclude that both dry and wet frequencies strongly depend on the cone deadrise angle, but their ratios are approximately constant in the interval $0 \leq \beta \leq 15^\circ$. Here $\beta = 0$ corresponds to the circular elastic plate, which is clamped at the centre and at the edge. The obtained results about weak dependence of the ratios of dry and wet frequencies on the cone deadrise angle are similar to the findings by Korobkin *et al.* (2023) for the ratios of dry and wet frequencies of two-dimensional floating complex elastic structures.

The frequencies of the three lowest dry modes of the cone with deadrise angle $\beta = 10^\circ$ were computed with the help of the finite-element structural solver ABAQUS by Malenica *et al.* (2022) as $\omega_1^{(d)}/2\pi = 247$ Hz, $\omega_2^{(d)}/2\pi = 334.6$ Hz and $\omega_3^{(d)}/2\pi = 475.9$ Hz. The frequencies $\omega_1^{(d)}/2\pi = 247.25$ Hz, $\omega_2^{(d)}/2\pi = 336.2$ Hz and $\omega_3^{(d)}/2\pi = 479$ Hz predicted by the present model, see figure 4(a), are very closed to the computed ones.

The shapes of the dry and wet modes of the elastic cone for case 2, as well as the shapes of the circular plate modes are shown in figure 5 for $n = 1, 2, 3$ and $n = 10$. It is seen that the higher modes are weakly dependent on the deadrise angle and the presence of the liquid in contact with the structure.

The eigenfrequencies of a conical shell strongly depend on the deadrise angle of the cone. Figure 4(a) shows that the lowest dry frequency $\omega_1^{(d)}/2\pi$ of the circular plate is 56.5 Hz and the frequencies of the conical shell with $\beta = 5^\circ$ and 10° are 141.5 and 247.25 Hz correspondingly. We conclude that a conical shell is much less flexible than an equivalent circular plate with the same elastic characteristics even for small deadrise angles. It is important to mentioned that dry and wet lowest modes of the cone, see figure 5, are not close to each other as is the case for two-dimensional problems of hydroelasticity, see Korobkin *et al.* (2023).

Water entry of an elastic conical shell

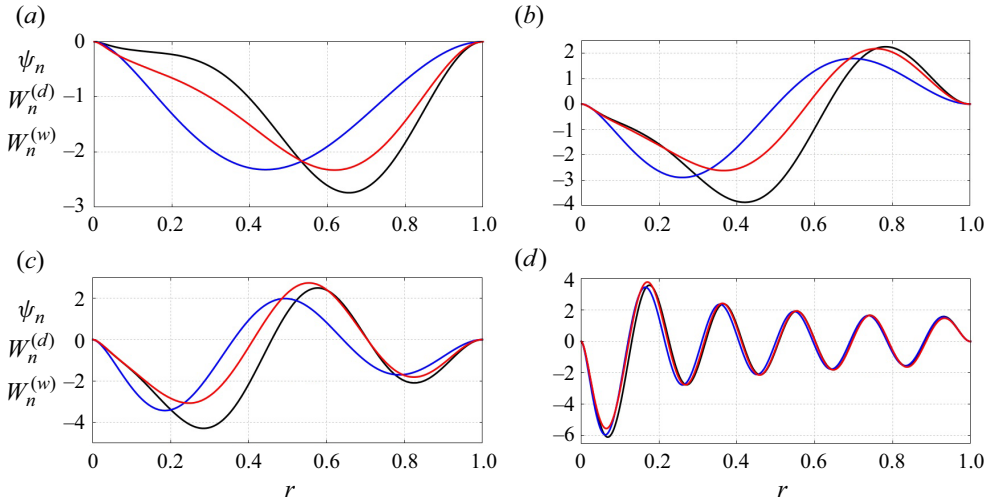


Figure 5. Shapes of the elastic modes in case 2 for $\beta = 10^\circ$ with $n = 1$ (a), $n = 2$ (b), $n = 3$ (c) and $n = 10$ (d). The blue lines are for dry modes $\psi_n(r)$ of equivalent circular plate, black lines are for dry modes $W_n^{(d)}(r)$ and red lines are for wet modes $W_n^{(w)}(r)$ of the conical shell.

4.2. Deflections and strains during the conical shell impact on water

Calculations are performed for case 1 to compare the deflections of the elastic cone within the Scolan model and the present model. Note that the results by Scolan (2004) are provided by the present model with $\delta = 0$. The system (3.19) and (3.20) is integrated with respect to the dimensionless radius of the wetted surface $a(t)$ using the Runge–Kutta fourth-order method with step $\Delta a = 10^{-4}$. The system is integrated with 8 and 20 modes to confirm convergence of the results in terms of the mode number. Difference of the functions $a(t)$ and $w(x, t)$ computed with 8 and 20 modes are small. Only results with 20 modes are shown in the following.

The dimensional radius, $a(t)$, of the wetted part of the elastic cone for case 1 is shown in figure 6(a) for $\delta = 0$ (circular elastic plate) and $\delta = 965.3$ (conical shell with deadrise angle of 6°). It is seen that the conical shell is less flexible than the circular plate, and the radius of the wetted part of the conical shell is close to the radius for the rigid cone, $a(t) = 4Vt/(\pi \sin \beta)$, shown by dashed line.

The dimensionless coefficients $b_1(t)$, $b_2(t)$, $b_3(t)$ in the series (3.5) for the normal displacements of the shell elements are shown in figure 6(b,d) correspondingly for $\delta = 0$ (blue lines) and for $\delta = 965.3$ (red lines). It is seen that the coefficient $b_1(t)$ of the lowest mode is larger for $\delta = 0$, but other coefficients with $\delta = 0$ are smaller than those with $\delta \neq 0$. Therefore, the total deflection of the conical shell is smaller than in the model by Scolan (2004). However, the contributions of the dry modes starting from the second one in the model by Scolan are higher than in the present model of conical shells.

Dimensional normal displacements of the cone at different time instants are shown in figure 7 for Scolan model, see figure 7(a), and the present model, figure 7(b). The scale of the normal displacement is $R \sin \beta = 1.338 \times 10^{-2}$ m for case 1, see (2.10a–d). The conical shell is much less deformed at the early stage. The maximum deflection of the shell is more than twice smaller than the deflection of an equivalent circular plate.

Calculations of the shell deflection in case 2 are performed with 20 modes and step of integration $da = 10^{-5}$ and with 8 modes and step of integration $da = 10^{-4}$ by

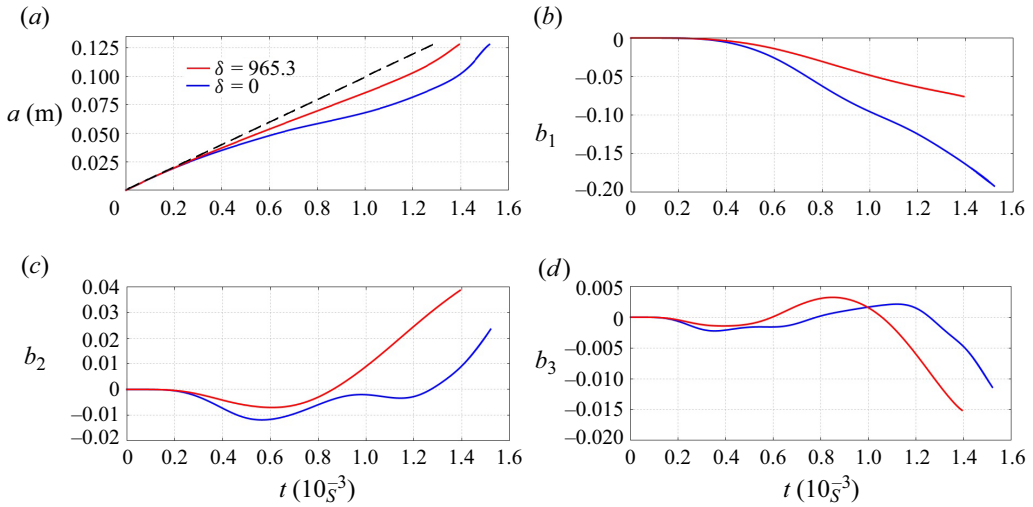


Figure 6. Comparison of the results within the Sclan model (blue lines) and the present model of conical shell (red lines): (a) dimensional radius of the wetted area $a(t)$, dashed line is for rigid cone; (b–d) coefficients $b_n(t)$ in the series (21).

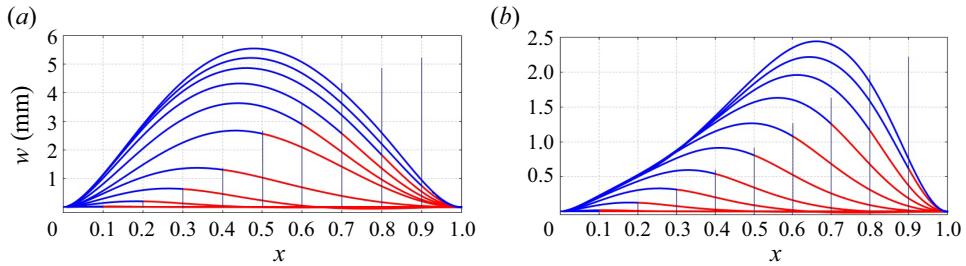


Figure 7. Normal dimensional displacement $w(x, t)$ of the circular plate (a) and the conical shell (b) for case 1 during the impact stage at time instants when $a_j/R = 0.1 \cdot j$, $1 \leq j \leq 10$. Displacement of the wetted parts of the structure are shown in blue and displacements of the dry parts are shown in red.

Runge–Kutta fourth-order method. The results with 20 modes and with 8 modes are very close. In the following, the normal displacements with 20 modes are shown for the impact speed 6 m s^{-1} (see figure 8a) and 12 m s^{-1} (see figure 8b). It is seen that double increase of the impact speed results in the increase of the maximum shell deflection more than four times.

There are two strain components for a conical shell, $\varepsilon_{xx}(x, t)$ and $\varepsilon_{\theta\theta}(x, t)$, as shown in figure 3 and (2.19a,b). The distributions of the membrane, $\varepsilon_{xx}^{(m)}(x, t)$ and $\varepsilon_{\theta\theta}^{(m)}(x, t)$, and bending, $\varepsilon_{xx}^{(b)}(x, t)$, $\varepsilon_{\theta\theta}^{(b)}(x, t)$, strains, see (2.20a,b), along the cone at different time instants are shown in figures 9(a) and 9(b) for case 2 with impact speed 12 m s^{-1} . Strain are given in microstrains (μs). We may conclude that the bending strains are greater than the membrane strains in the radial direction, but the membrane strains are higher than the bending strains in the azimuthal direction. All strain components are of about the same order. The maximum strains are achieved at the edge of the cone because of bending. The strain distributions on the inner and outer surfaces of the cone are shown in figures 9(c)

Water entry of an elastic conical shell

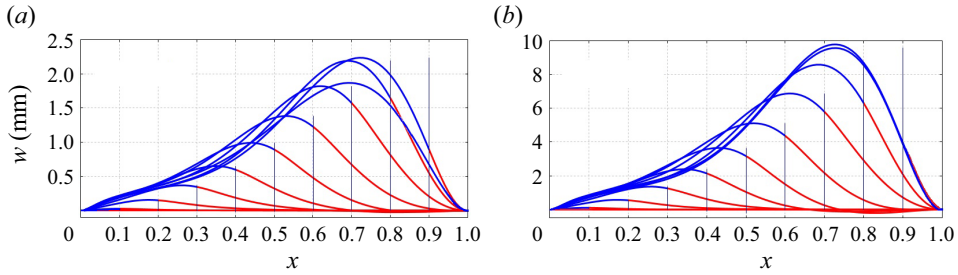


Figure 8. Normal dimensional displacement $w(x, t)$ of the conical shell for case 2 and impact speed $V = 6 \text{ m s}^{-1}$ (a) and $V = 12 \text{ m s}^{-1}$ (b) during the impact stage at time instants when $a_j/R = 0.1 \cdot j$, $1 \leq j \leq 10$. Displacement of the wetted parts of the structure are shown in blue and displacements of the dry parts are shown in red.

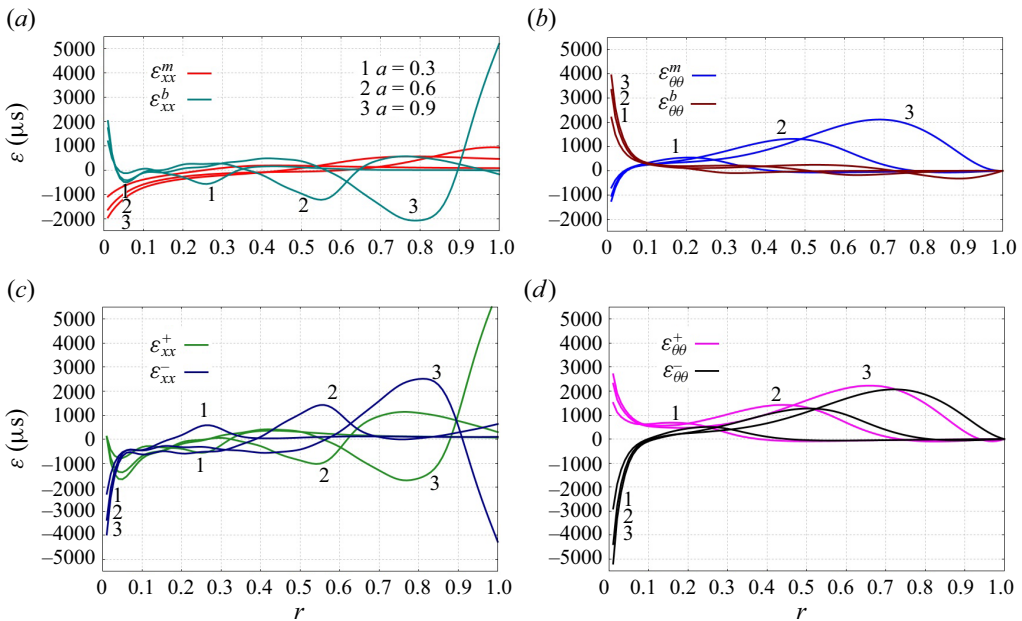


Figure 9. Distributions of the strain components at the three time instants corresponding to the radius of the contact region $a(t) = 0.3$ (curve 1), $a(t) = 0.6$ (curve 2) and $a(t) = 0.9$ (curve 3): (a) radial membrane and bending strain components; (b) azimuthal membrane and bending strain components; radial (c) and azimuthal (d) strains along the inner (-) and outer (+) surfaces of the cone, $V = 12 \text{ m s}^{-1}$. The strains (in microstrains) are shown for case 2.

and 9(d). Note that the strains are singular at the tip of the cone, see the discussions in the last paragraph of § 2.

Strain components at two points of conical shell, $x = 0.5$ and $x = 0.75$, are shown as functions of the dimensionless time \tilde{t} in figure 10. This figure indicates that all components of the strain should be evaluated during both, the impact and penetration stages to find the maximum strain at a certain point of the conical shell. The strain are unbounded at the tip of the cone, $x = 0$. However, the elastic displacement near the tip are small and a vicinity of the tip can be treated as rigid. A better way of dealing with the strain singularity is to consider a frustum of a cone, where part near the vertex is rigid and elastic shell

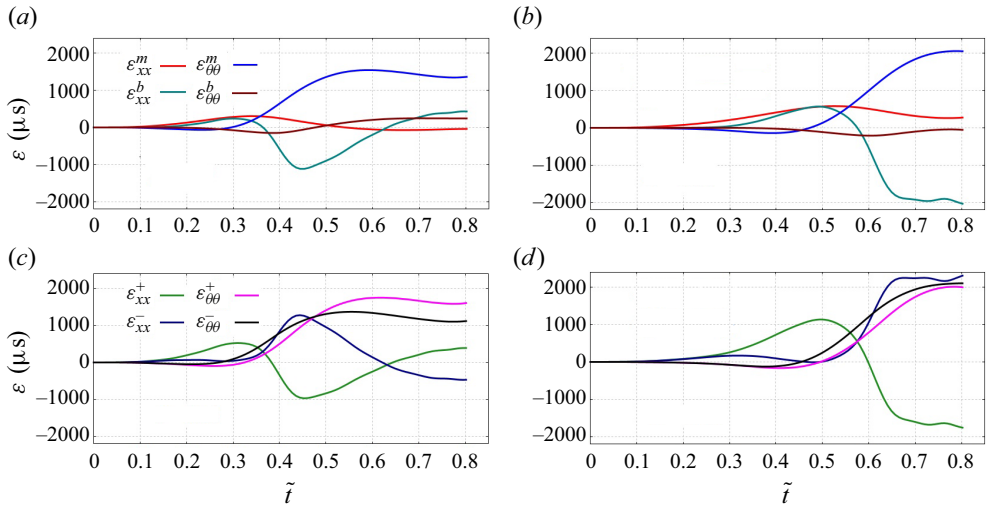


Figure 10. Radial and azimuthal strains (in microstrains) as functions of dimensionless time at dimensionless distances $x = 0.5$ and $x = 0.75$ from the cone tip for case 2 with impact speed 12 m s^{-1} . Bending and membrane components $x = 0.5$ (a) and $x = 0.75$ (b). Strains at the inner (–) and outer (+) surface of the cone, $x = 0.5$ (c) and $x = 0.75$ (d). Time scale is 14.5 ms.

corresponds to $R_m < x < R$. Elastic shell is clamped to the rigid part near the vertex at $x = R_m$.

4.3. Hydrodynamic pressure

It was discussed in § 3.3 that the hydrodynamic loads acting on the conical shell during water impact are difficult to compute and measure. However, the loads should be estimated to guarantee that they do not drop to the level where the liquid starts cavitating. In the case of very low pressures, the hydrodynamic model should be changed to include cavitation effects.

The dimensionless pressure distributions shown in figure 11 for four time instants with $a = 0.2, 0.6, 0.8$ and 1 are calculated by series (3.33) (blue lines) and by the series with improved convergence (3.41) (red lines) for Case 2 with 20 modes and speed of impact 1 m s^{-1} . The series (3.33) gives the pressure in the contact region, $0 < r < a$, as well as in the dry part of the cone, where $a < r < 1$ and $p(r, 0, t) = 0$. The series (3.33) does not reproduce the square-root singularity of the pressure at $r = a(t)$. The pressure distributions provided by formula (3.41) with improved convergence of the series are smooth, but some oscillations of the pressure occur due to elastic vibration of the shell. Note that the modes $\psi_n(r)$ in (3.5) are such that $\psi_n(0) = \psi_n(1) = 0$, see (3.1a,b). Correspondingly, the series (3.33) incorrectly gives $p(0, 0, t) = p(1, 0, t) = 0$ for an any finite number of retained terms.

The pressure distributions for case 2 and impact speed 6 m s^{-1} are shown in figure 12(a) in the dimensionless variables at five time instants, which corresponds to $a = 0.2, 0.4, 0.6, 0.8$ and 1 . There are four types of lines in this figure. The pressures by formulae (3.33) and (3.41) are shown by green and red lines correspondingly. The black lines are for the pressures acting on the equivalent rigid cone. The blue lines show the differences between the elastic and rigid cone pressures. It is seen that the elastic and rigid pressures are different only at the end of the impact stage. Within the rigid cone model, the pressure

Water entry of an elastic conical shell

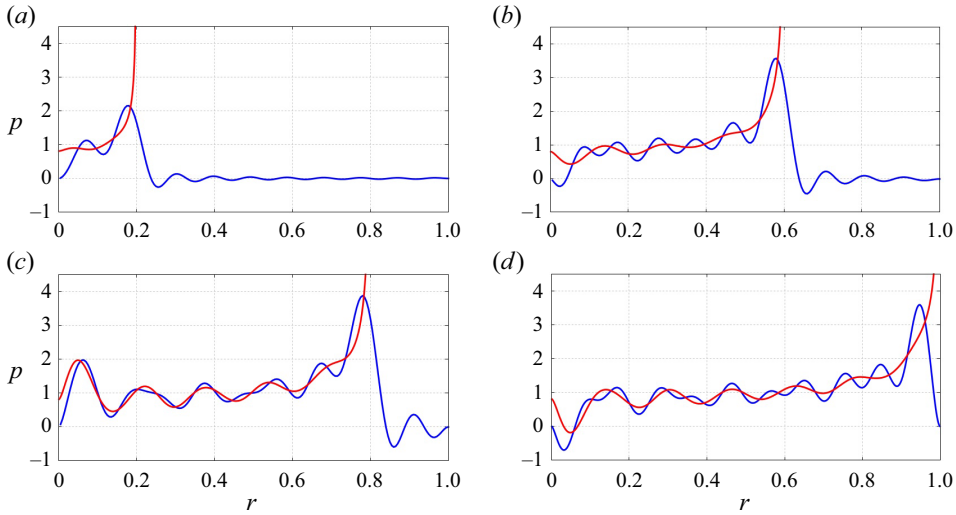


Figure 11. Hydrodynamic pressure distributions in case 2 with entry speed 1 m s^{-1} , calculated by series (3.33) (blue lines) and by the series with improved convergence (3.41) (red lines) at time instants, when $a = 0.2$ (a), $a = 0.6$ (b), $a = 0.8$ (c) and $a = 1$ (d), in dimensionless variables.

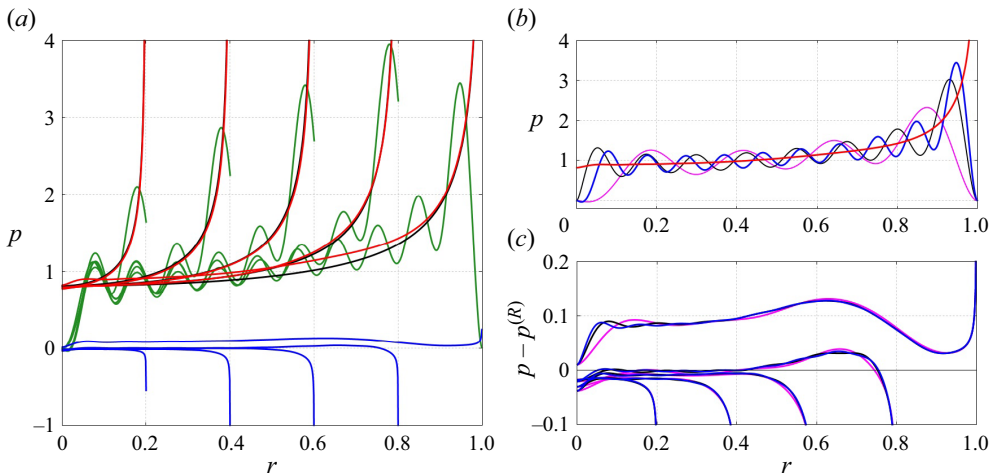


Figure 12. (a) Dimensionless pressure distributions in case 2 with entry speed 6 m s^{-1} calculated by series (3.33) (green lines), by formula (3.41) (red lines) and without account for cone elasticity (black lines). The difference between elastic and rigid pressure are shown by blue lines. (b) Hydrodynamic pressure given by the series (41) at the end of the impact stage with 8 (magenta), 15 (black) and 20 (blue) retained modes compared with the pressure provided by (3.41) with 20 modes. (c) The difference between the elastic (3.41) and rigid (3.43) pressures, calculated with 8 (magenta), 15 (black) and 20 (blue) modes.

$p^{(R)}(r, 0, t)$ is given by (3.43) where the radius $a(t)$ is calculated without account for cone elasticity. The blue lines show the differences $p - p^{(R)}$ between the elastic and rigid pressures for the same values of the radius a . It is interesting that the elastic pressure can be higher than the rigid pressure in some places.

The convergence of the pressure given by (3.33) to the pressure provided by (3.41) with increase of the number of retained modes is demonstrated in figure 12(b) for the same

conditions as in figure 12(a), but only at the end of the impact stage when $a(t) = 1$. The pressure distributions by the series (3.33) with 8 modes (magenta), 15 modes (black) and 20 modes (blue) converge to the pressure predicted by (3.41) (red line) but very slowly.

The differences between the elastic (3.41) and rigid (3.43) pressures $p - p^{(R)}$, which are shown in figure 12(a) by blue lines, are shown now with 8 (magenta), 15 modes (black) and 20 modes (blue) modes retained in (3.41) in figure 12(c) for 5 time instants as in figure 12(a). This figure demonstrates fast convergence of the series (3.41) with increase of the retained modes. It is seen that the elastic pressure (3.41) is smaller than the rigid pressure (3.43) (the difference is negative) for $a = 0.2, 0.4$ and 0.6 , but at the end of the impact stage elastic pressure is higher than the rigid pressure. This effect can be caused by deflection of the elastic cone, when the local deadrise angle at $x = a(t)$ increases initially decreasing the hydrodynamic pressure, but then decreases at the end of the impact stage increasing the impact pressure.

4.4. Convergence of the numerical solution

Convergence issues with respect to the number of the retained modes N were addressed qualitatively in §§ 4.2 and 4.3. In the present section, the convergence issues are addressed quantitatively for local quantities, such as deflection, strain and pressure distributions along the wetted part of the conical shell, at a certain time instant. All results in the following are given for case 2 with impact speed $V = 6 \text{ m s}^{-1}$ for the normal displacements of the shell elements and hydrodynamic pressures, and $V = 12 \text{ m s}^{-1}$ for both radial and azimuthal strains on the outer surface of the shell. The deflection, strain and pressure distributions are compared at the time instant t^* , when the dimensionless radius of wetted part of the elastic cone is equal to 0.9, $a(t^*) = 0.9$.

The relative differences in percentage of the normal displacements of shell elements computed with N retained modes, $w_N(x, t^*)$, and 20 modes, $w_{20}(x, t^*)$, at time t^* ,

$$\Delta^* w(x, t^*) = \frac{w_N(x, t^*) - w_{20}(x, t^*)}{\max_{0 \leq x \leq 1}(w_{20}(x, t^*))} \cdot 100 \%, \quad (4.3)$$

are shown in figure 13(a) for $N = 5, 10$ and 15 . The deflection $w_{20}(x, t^*)$ is shown in figure 8(a) by the line with absolute maximum, which is achieved at $x = 0.72$. It is seen that relative difference between $w_{10}(x, t^*)$ and $w_{20}(x, t^*)$ is less than 0.5 % (see the magenta line). The convergence of normal displacements $w_N(x, t^*)$ with increase of the number of the retained modes N is clear from figure 13(a).

The relative differences in percentage of the strain $\varepsilon_{xx}^+(x, t)$ along the cone generator and the strain $\varepsilon_{\theta\theta}^+(x, t)$ in the angular azimuthal direction (see figure 3) computed for the outer surface of the conical shell with N retained modes, $\varepsilon_{N,xx}^+(x, t)$ and $\varepsilon_{N,\theta\theta}^+(x, t)$, at time instant t_*

$$\Delta^* \varepsilon_{xx}^+(x, t^*) = \frac{\varepsilon_{N,xx}^+(x, t^*) - \varepsilon_{20,xx}^+(x, t^*)}{\varepsilon_{20,xx}^+(1, t^*)} \cdot 100 \%, \quad (4.4)$$

$$\Delta^* \varepsilon_{\theta\theta}^+(x, t^*) = \frac{\varepsilon_{N,\theta\theta}^+(x, t^*) - \varepsilon_{20,\theta\theta}^+(x, t^*)}{\varepsilon_{20,\theta\theta}^+(0.66, t^*)} \cdot 100 \%, \quad (4.5)$$

are shown in figures 13(b) and 13(c) correspondingly for $N = 5, 10$ and 15 . Note that strains are unbounded at $x = 0$ and, therefore, convergence of the strains should be considered out of a vicinity of the cone vertex. The denominators $\varepsilon_{20,xx}^+(1, t^*)$ and

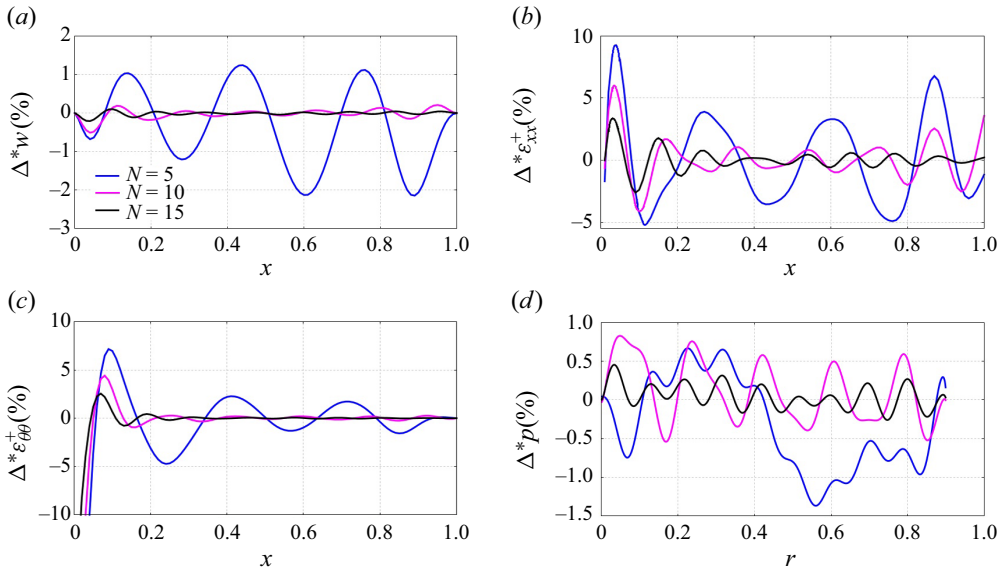


Figure 13. Relative differences of the normal displacement (4.3) (a), radial strains (4.4) (b), azimuthal strains (4.5) (c) and impact loads (4.6) (d) calculated with $N = 5$ (blue lines), $N = 10$ (magenta lines) and $N = 15$ (black lines) with respect to the results, calculated with 20 modes retained in the corresponding series, at time instant t_* , when 90% of the cone generator is wetted.

$\varepsilon_{20,\theta\theta}^+(0.66, t^*)$ in (4.4) and (4.5) are the extreme of the corresponding strains outside the vicinities of the vertex. It is seen that relative differences between $\varepsilon_{20,xx}^+(x, t^*)$ and $\varepsilon_{15,xx}^+(x, t^*)$, and between $\varepsilon_{20,\theta\theta}^+(x, t^*)$ and $\varepsilon_{15,\theta\theta}^+(x, t^*)$, are less than 2% for $0.1 < x < 1$.

It is well known that convergence of the strains with respect to the number of retained modes is slower than convergence of the deflections, because strains are computed as second derivatives of the deflections with respect to the radial coordinate x . The terms in the series (3.5) for the normal displacement $w(x, t)$ are at the order $O(b_n \psi_n) = O(b_n)$ because the normalised modes (3.3) are of order $O(1)$. The second derivatives $\psi_n''(r)$ are of order $O(n^2)$ for $0 < r < 1$. Therefore, the series for the strains are with terms of order $O(n^2 b_n(t))$ as $n \rightarrow \infty$. From this analysis, we may conclude that the corresponding series for hydrodynamic pressure, which follows from the shell equations (2.4) and (2.5) and series (3.6) are with terms of order $O(n^4 b_n(t))$ as $n \rightarrow \infty$. The convergence of such series for the hydrodynamic pressure to the pressure provided by the series with improved convergence (3.41) is shown in figure 12(b), which demonstrates that the convergence is not acceptable for practical estimates of impact loads.

The relative differences in percentage of the pressure given by (3.41) with N retained modes in (3.41) and (3.40), $p_N(x, t^*)$, and 20 modes, $p_{20}(x, t^*)$,

$$\Delta^* p(x, t^*) = \frac{p_N(x, t^*) - p_{20}(x, t^*)}{p_{20}(x, t^*)} \cdot 100 \%, \tag{4.6}$$

are shown in figure 13(d) for $N = 5, 10$ and 15 at time instant t^* when $a(t^*) = 0.9$. It is seen that the relative difference between $p_{15}(x, t^*)$ and $p_{20}(x, t^*)$ is less than 0.5%. This result confirms that the accuracy of the formula (3.41) for the impact loads is comparable with the accuracy of the series for the shell displacements.

5. Conclusion

The deflections and strains of a conical shell with a small deadrise angle, which enters the water surface with a constant speed, have been investigated within the most general linear theory of conical shells and the Wagner model of hydrodynamic impact loads. The water was of infinite depth, and its flow was assumed to be axisymmetric and potential. The hydrodynamic loads have been calculated as well separating the singular part of the load and using series with improved convergence.

The wet and dry modes of natural vibrations of the conical shells together with their corresponding frequencies were calculated and compared with numerical results by Malenica *et al.* (2022). The wet and dry modes were presented as superpositions of the natural dry modes of a circular elastic plate with the radius equal to the length of the cone generator and the same edge conditions as for the original cone.

The circular elastic plate clamped at its edge and at its centre was used by Scolan (2004) as a structural model of an elastic cone with small deadrise angle. Conditions under which this approximation of a conical shell is justified have been derived in § 2.

It was shown that the ratios of wet and dry frequencies of a conical shell are weakly dependent on the cone deadrise angle, even both frequencies monotonically increase with increase of the deadrise angle.

It was shown that lowest dry and wet modes are not close one to another in contrast with the case of two-dimensional floating elastic structures. However, the shapes of high-frequency dry and wet modes of a conical shell are very close one to another and to the corresponding shapes of the dry modes of a circular elastic plate.

The hydrodynamic part of the problem is the same as in the study by Scolan (2004) because the structural normal modes are the same as in present study, they are the modes of a circular plate. However, the structural part of the present study is different from the structural model of the elastic cone employed by Scolan.

Comparison of the present results for a conical shell and the results by Scolan within the flat-disc approximation of the cone confirmed that a conical shell is much less flexible than the 'equivalent' circular plate, deflections of conical shells are smaller than the deflections within the flat-disc approximation, but higher modes are better pronounced for a conical shell than for circular plate.

The strains in a conical shell are made of membrane strains and bending strains. All strain components are of similar order. They should be evaluated at each point of the cone to conclude about a possible damage to the conical shell during water impact. For a complete cone, the strains are unbounded at the cone vertex, but bounded for a frustum of the cone with part of the cone near the vertex being rigid.

The hydrodynamic pressures acting on an elastic cone entering the water at a constant speed were shown to be smaller than the pressures acting on an equivalent rigid cone during the early stage of impact but then they become higher than the pressures for the rigid cone closer to the end of the impact stage, when the cone is completely wetted.

The normal mode method in hydroelastic problems, which employs normal modes of a simplified structure, has been used in the past for two-dimensional slamming problems (see Korobkin *et al.* 2023 and references there). In the present paper, this approach is applied successfully to axisymmetric slamming problems for the first time. This approach can be applied to the problem of a spherical shell impact on water without any difficulties.

Deflections and strains were calculated only for the impact stage, when the elastic cone is partly wetted. The nonlinear system (3.19) and (3.37) was integrated in time. During the next, penetration stage, when the cone is completely wetted and continues to penetrate into the liquid, the linear system (3.22) with constant coefficients should be integrated.

Numerical analysis of the penetration stage was not performed in this paper. This analysis is required to determine maximum deflection of the shell and maximum strain at certain points of the structure. This will be done in a future paper by the authors where the predictions by the semi-analytical model of three-dimensional hydroelastic slamming will be compared with the computational results using OpenFoam and FEM solvers. The predictions by the quasi-static model, where the hydrodynamic loads are calculated for the rigid cone and applied to the static structural model, will be also compared with the present results obtained by the simplified dynamic and coupled model.

Impact on water by elastic panels with double curvature is still a challenging problem. Even in a simple case, where the edge of the panel is circular, $x^2 + y^2 < R^2$, but the panel is ellipsoidal with the initial shape $z = x^2/(2r_x) + y^2/(2r_y)$. We can use the modes of the circular elastic plate with corresponding edge conditions; however, the hydrodynamic part of the problem is truly three-dimensional with the contact line between the deformed panel and the disturbed water being a three-dimensional curve, which should be determined as part of the solution. Therefore, for water impact by an elastic panel with double curvature, the main difficulty are due to three-dimensionality of the flow caused by impact and coupling this flow with two-dimensional deflection of the panel. In terms of numerical difficulties with three-dimensional problems of hydroelastic slamming within the Wagner model of water impact, one should mention that the number of natural modes required for convergence in 3D problems is much higher than in similar 2D coupled problems (see Korobkin & Khabakhpasheva 2022).

Acknowledgements. We kindly thank the anonymous reviewers for their constructive comments.

Funding. T.Kh. and A.K. gratefully acknowledge the financial support received from the University of East Anglia through Pro-Vice-Chancellor Impact Fund and Associate Dean Research Impact Fund within the grant ‘Wave Slamming’.

Declaration of interests. The authors report no conflict of interest.

Data availability. The data that support the findings of this study are available from the corresponding author, upon reasonable request.

Author ORCIDs.

 T.I. Khabakhpasheva <https://orcid.org/0000-0003-4058-0508>;

 A.A. Korobkin <https://orcid.org/0000-0003-3605-8450>;

 S. Malenica <https://orcid.org/0009-0002-0122-1465>.

REFERENCES

- BALDWIN, J.L. 1971 Vertical water entry of cones. Naval Ordnance Lab. White Oak. MD.
- CAUSIN, P., GERBEAU, J.F. & NOBILE, F. 2005 Added-mass effect in the design of partitioned algorithms for fluid-structure problems. *Comput. Meth. Appl. Mech. Engng* **194** (42–44), 4506–4527.
- CHUANG, S.L. & MILNE, D.T. 1971 Drop tests of cones to investigate the three-dimensional effects of slamming. David W. Taylor Naval Ship Research and Development Center. Bethesda. MD.
- COURANT, R., SHIFFMAN, M. & SPENCER, D.C. 1945 The force of impact on a sphere striking a water surface. New York Univ. Courant Inst Of Mathematical Sciences. NY.
- DONGUY, B., PESEUX, B., GORNET, L. & FONTAINE, E. 2001 Three-dimensional hydroelastic water entry: preliminary results. In *Int. Ocean and Polar Eng. Conf.* International Society of Offshore and Polar Engineers, Cupertino, CA, 2001.
- FALTINSEN, O.M. 1999 Water entry of a wedge by hydroelastic orthotropic plate theory. *J. Ship Res.* **43** (3), 180–193.
- FALTINSEN, O.M. 2000 Hydroelastic slamming. *J. Mar. Sci. Technol.* **5**, 49–65.

- GAZZOLA, T., KOROBKIN, A.A., MALENICA, S. & SCOLAN, Y.-M. 2005 Three-dimensional Wagner problem using variational inequalities. In *Pros. 20th Int. Workshop on Water Waves and Floating Bodies* (ed. J. Grue). University of Oslo, Norway.
- GAZZOLA, T. & DE LAUZON, J. 2008 Three-dimensionnal hydroelastic Wagner impact using variational inequalities. In *Proc. 8th Int. Conf. on Hydrodynamics* (ed. P. Ferrant & X.B. Chen). ICHD 2006 Local Organizing Committee, La Chapelle sur Erdre, France.
- GRIGOLYUK, E.I. & GORSHKOV, A.G. 1971 Impact of a conical shell against water. *Dokl. Akad. Nauk* **198** (2), 313–315.
- HOWISON, S.D., OCKENDON, J.R. & WILSON, S.K. 1991 Incompressible water-entry problems at small deadrise angles. *J. Fluid Mech.* **222**, 215–230.
- KHABAKHPASHEVA, T. & KOROBKIN, A.A. 2013 Elastic wedge impact onto a liquid surface: Wagner's solution and approximate models. *J. Fluids Struct.* **36**, 32–49.
- KOROBKIN, A.A. 1982 Formulation of penetration problem as a variational inequality. *Din. Splashnoi Sredy* **58**, 73–79.
- KOROBKIN, A.A. & Khabakhpasheva, T.I. 2006 Regular wave impact onto an elastic plate. *J. Engng Maths* **55** (1–4), 127–150.
- KOROBKIN, A.A. & Khabakhpasheva, T. 2022 Three-dimensional hydroelastic impact onto a floating circular plate. In *Proc. of 9th Int. Conf. on Hydroelasticity in Marine Tech.* (ed. D. Dessi & A. Iafrazi), pp. 79–88. Rome, Italy.
- KOROBKIN, A.A., Khabakhpasheva, T.I. & Shishmarev, K.A. 2023 Eigen modes and added-mass matrices of hydroelastic vibrations of complex structures. *J. Fluid Mech.* **970**, A14.
- LEISSA, A.W. 1973 Vibration of shells. NASA SP-288.
- LOGVINOVICH, G.V. 1972 Hydrodynamics of free-boundary flows. NASA TT F-658. Israel Prog. Sci. Transl. US Dep. Commerce, Natl. Tech. Inf. Serv.
- MALENICA, S., GATIN, I., SENG, S., JAGITE, G., DIEBOLD, L., Khabakhpasheva, T. & KOROBKIN, A.A. 2021 Some aspects of the local hydro-structure interactions during hydrodynamic impacts. In *23rd Numerical Towing Tank Symposium* (ed. O. El Moctar). Curran Associates, Inc.
- MALENICA, S., SENG, S., DIEBOLD, L., SCOLAN, Y.M., KOROBKIN, A.A. & Khabakhpasheva, T. 2022 On three dimensional hydroelastic impact. In *Proc. of 9th Int. Conf. on Hydroelasticity in Marine Tech.* (ed. D. Dessi & A. Iafrazi), pp. 89–100. Rome, Italy.
- PEGG, M., PURVIS, R. & KOROBKIN, A. 2018 Droplet impact onto an elastic plate: a new mechanism for splashing. *J. Fluid Mech.* **839**, 561–593.
- SCOLAN, Y.M. 2004 Hydroelastic behaviour of a conical shell impacting on a quiescent-free surface of an incompressible liquid. *J. Sound Vib.* **277** (1–2), 163–203.
- SCOLAN, Y.M. & KOROBKIN, A.A. 2001 Three-dimensional theory of water impact. Part 1. Inverse Wagner problem. *J. Fluid Mech.* **440**, 293–326.
- SENG, S. 2013 Slamming and whipping analysis of ships. PhD thesis, Technical University of Denmark.
- SENG, S., JENSEN, J.J. & MALENICA, Š. 2014 Global hydroelastic model for springing and whipping based on a free-surface CFD code (OpenFOAM). *Intl J. Naval Arch. Ocean Engng* **6** (4), 1024–1040.
- SHIFFMAN, M. & SPENCER, D.C. 1951 The force of impact on a cone striking a water surface (vertical entry). *Commun. Pure Appl. Maths* **4** (4), 379–417.
- SOEDEL, W. 2004 *Vibrations of Shells and Plates*. CRC Press.
- SUN, H. & FALTINSEN, O.M. 2006 Water impact of horizontal circular cylinders and cylindrical shells. *Appl. Ocean Res.* **28** (5), 299–311.
- TASSIN, A., JACQUES, N., ALAOU, A.E.M., NEME, A. & LEBLE, B. 2012 Hydrodynamic loads during water impact of three-dimensional solids: modelling and experiments. *J. Fluids Struct.* **28**, 211–231.
- WAGNER, H. 1932 Über stoss- und gleitvorgänge an der oberfläche von flüssigkeiten. *Z. Angew. Math. Mech.* **12** (4), 193–215.
- WAN, F.Y. 1970 On the equations of the linear theory of elastic conical shells. *Stud. Appl. Maths* **49** (1), 69–83.